Inorganic Chemistry

Article

pubs.acs.org/IC

Reactivity of Rhodium(I) Complexes Bearing Nitrogen-Containing Ligands toward CH_3I: Synthesis and Full Characterization of Neutral *cis*-$[RhX(CO)_2(L)]$ and Acetyl $[RhI(\mu\text{-}I)(COMe)(CO)(L)]_2$ Complexes

Romain J. Adcock, Duc Hanh Nguyen,* Sonia Ladeira, Carole Le Berre, Philippe Serp, and Philippe Kalck*

Laboratoire de Chimie de Coordination UPR CNRS 8241, composante ENSIACET, Université de Toulouse, UPS-INP-LCC, 4 allée Emile Monso, BP 44362, 31030 Toulouse Cedex 4, France

Supporting Information

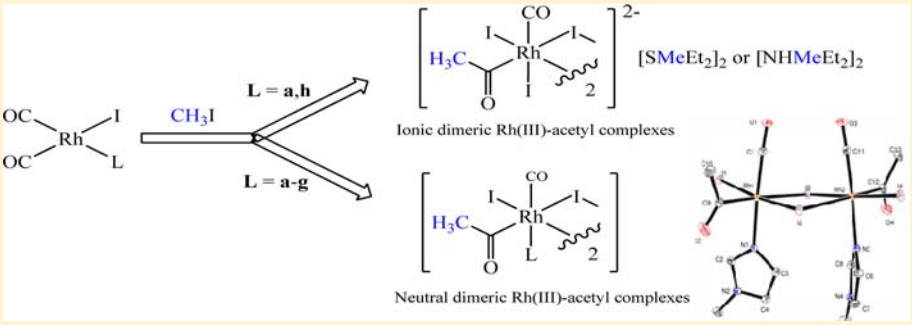

ABSTRACT: The neutral rhodium(I) square-planar complexes $[RhX(CO)_2(L)]$ [X = Cl (**3**), I (**4**)] bearing a nitrogen-containing ligand L [diethylamine (**a**), triethylamine (**b**), imidazole (**c**), 1-methylimidazole (**d**), pyrazole (**e**), 1-methylpyrazole (**f**), 3,5-dimethylpyrazole (**g**)] are straightforwardly obtained from L and $[Rh(\mu\text{-}X)(CO)_2]_2$ [X = Cl (**1**), I (**2**)] precursors. The synthesis is extended to the diethylsulfide ligand **h** for **3h** and **4h**. According to the CO stretching frequency of **3** and **4**, the ranking of the electronic density on the rhodium center follows the order **b** > **a** ≈ **d** > **c** > **g** > **f** ≈ **h** > **e**. The X-ray molecular structures of **3a**, **3d**−**3f**, **4a**, and **4d**−**4f** were determined. Results from variable-temperature ^1H and $^{13}C\{^1H\}$ NMR experiments suggest a fluxional associative ligand exchange for **4c**−**4h** and a supplementary hydrogen-exchange process in **4e** and **4g**. The oxidative addition reaction of CH_3I to complexes **4c**−**4g** affords the neutral dimeric iodo-bridged acetylrhodium(III) complexes $[RhI(\mu\text{-}I)(COCH_3)(CO)(L)]_2$ (**6c**−**6g**) in very good isolated yields, whereas **4a** gives a mixture of neutral **6a** and dianionic $[RhI_2(\mu\text{-}I)(COCH_3)(CO)][NHMeEt_2]_2$ and **4h** exclusively provides the analogue dianionic complex with $[SMeEt_2]^+$ as the counterion. X-ray molecular structures for $\mathbf{6d_2}$ and **6e** reveal that the two apical CO ligands are in mutual cis positions, as are the two apical **d** and **e** ligands, whereas isomer $\mathbf{6d_1}$ is centrosymmetric. Further reactions of **6d** and **6e** with CO or ligand **e** gave quantitatively the monomeric complexes $[RhI_2(COCH_3)(CO)_2(\mathbf{d})]$ (**7d**) and $[RhI_2(COCH_3)(CO)(\mathbf{e})_2]$ (**8e**), respectively, as confirmed by their X-ray structures. The initial rate of CH_3I oxidative addition to **4** as determined by IR monitoring is dependent on the nature of the nitrogen-containing ligand. For **4a** and **4h**, reaction rates similar to those of the well-known rhodium anionic $[RhI_2(CO)_2]^-$ species are observed and are consistent with the formation of this intermediate species through methylation of the **a** and **h** ligands. The reaction rates are reduced significantly when using imidazole and pyrazole ligands and involve the direct oxidative addition of CH_3I to the neutral complexes **4c**−**4g**. Complexes **4c** and **4d** react around 5−10 times faster than **4e**−**4g** mainly because of electronic effects. The lowest reactivity of **4f** toward CH_3I is attributed to the steric effect of the coordinated ligand, as supported by the X-ray structure.

INTRODUCTION

Methanol carbonylation based on rhodium or iridium complexes to manufacture around 80% of the 9×10^6 metric tons of acetic acid still represents one of the most successful industrial applications of homogeneous catalysis.[1] The anionic catalytic cycle is well established for the rhodium-catalyzed process, which involves *cis*-$[RhI_2(CO)_2]^-$ as the active species. The nucleophilic attack of *cis*-$[RhI_2(CO)_2]^-$ on CH_3I to form $[RhI_3(CH_3)(CO)_2]^-$ is the rate-limiting step, which is followed by the *cis*-CO migratory insertion to produce the corresponding acetylrhodium(III) complex $[RhI_3(CH_3CO)(CO)]^-$. This latter species further reacts with CO to provide the six-coordinate complex $[RhI_3(CH_3CO)(CO)_2]^-$, upon which takes place the classically proposed reductive elimination of CH_3COI and/or the substitution of I^- by an acetate ligand, followed by reductive elimination of acetic anhydride, with both products being immediately hydrolyzed to acetic acid.[2]

Received: September 12, 2011
Published: July 30, 2012

   dx.doi.org/10.1021/ic2019988 | *Inorg. Chem.* 2012, 51, 8670−8685

Significant research efforts are still performed to improve the rhodium catalyst activity and stability, particularly by tuning the electron density brought to the metal center by the appropriate ligand for promoting the rate of the kinetically limiting oxidative addition step. In this context, numerous rhodium complexes have been synthesized involving monodentate or hemilabile bidentate ligands, most of which contain a phosphorus atom.[3] However, such good electron-donating ligands generally retard CO insertion.

On the other hand, steric effects must also be considered during tailoring of the electron-donating character of a ligand. Indeed, the oxidative addition reaction rate can be reduced significantly using sterically hindered ligands, as observed for some carbene ligands.[4] Similarly, bulky ligands may impact the methylrhodium(III) complex lability, which results in back reductive elimination, despite their strong electron-donating ability, as shown for P,C,P[5] or P,N,P[6] pincer ligands. Nitrogen-containing ligands such as diimines,[7] pyridine,[3b] and its derivatives[8] have also been investigated. Very recently, Britovsek et al. have reported rhodium complexes bearing chelating bipyridine ligands with proximate acidic or basic functionalities for methyl acetate carbonylation reaction.[9]

In order to further understand the impact of ligands on the catalytic activity of rhodium complexes in methanol carbonylation, a synthetic strategy was defined by introducing donating monodentate nitrogen-containing ligands in the coordination sphere of the metal center to form neutral complexes $[RhI(CO)_2(L)]$ (**4**) with moderate steric hindrance. To the best of our knowledge, neither these iodo complexes nor their reactivity toward CH_3I have been reported, although several chloro **3** analogues have been well characterized with aliphatic[10] and heterocyclic ligands such as imidazole[11] or pyrazole.[12] The present study describes the synthesis and full characterization of **4** together with chloro analogues **3** to compare electronic and geometric features. Also, attention is focused on the reactivity of **4** toward CH_3I, leading to the corresponding neutral and/or ionic dimeric acetylrhodium(III) species, which have been structurally characterized. This reactivity has been evaluated in terms of electronic and steric contributions of the nitrogen-containing ligands. The oxidative addition of CH_3I to **4a** and **4h** is approximately as fast as that of the well-known $[RhI_2(CO)_2]^-$ species[13] and is consistent with the formation of this anionic rhodium(I) intermediate species, resulting from methylation of the **a** and **h** ligands. The reaction rates are reduced significantly when using imidazole and pyrazole ligands and involve the direct oxidative addition of CH_3I to the neutral complexes **4c**–**4g**.

RESULTS AND DISCUSSION

Synthesis and Characterization of Chlororhodium(I) Complexes $[RhCl(CO)_2(L)]$ (3). The reaction of 1 mol equiv of the starting rhodium precursor $[Rh(\mu\text{-}Cl)(CO)_2]_2$ (**1**) with 2 equiv of the nitrogen-containing ligand L (L = **a**–**h**) in dichloromethane at room temperature quantitatively afforded the neutral complexes *cis*-**3a**–**3h**, respectively, which are moderately air- and moisture-stable (Scheme 1). These compounds have been fully characterized by Fourier transform infrared (FT-IR), multinuclear NMR spectroscopy, mass spectrometry, elemental analyses, and single-crystal X-ray crystallography. Because attempts to isolate complex **3b** in the solid state were unsuccessful, **3b** was only characterized in situ by FT-IR.

IR data relevant to the characteristic ν_{CO} stretching frequencies of **3** in CH_2Cl_2 are displayed in Table 1. As

Scheme 1. General Pathway for the Synthesis of *cis*-$[Rh(X)(CO)_2(L)]$ [X = Cl (3), I (4)]

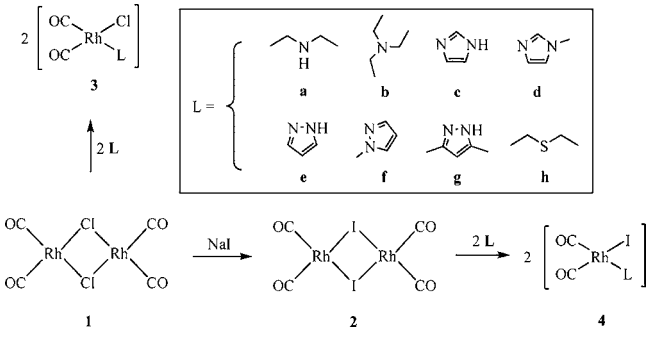

Table 1. IR Carbonyl Stretching Frequencies in 3

complex	$\nu_{CO}(CH_2Cl_2)$, cm^{-1}	$\Delta\nu_{CO}$, cm^{-1}	$\nu_{av(CO)}$, cm^{-1}	$pK_a(L)$
3a	2085.0, 2007.0	77.9	2046.0	10.84
3b	2084.1, 2004.7	79.4	2044.4	10.75
3c	2085.6, 2009.6	76.0	2047.6	6.95
3d	2084.2, 2008.3	75.9	2046.3	7.13
3e	2089.9, 2017.3	72.6	2053.6	2.52
3f	2089.7, 2015.5	74.2	2052.6	2.09
3g	2087.9, 2013.9	74.0	2050.9	4.12
3h	2091.0, 2014.9	76.1	2053.0	

expected, two bands of similar intensity are observed in the carbonyl region, illustrating typical behavior of CO ligands in mutual cis positions in a square-planar environment. The value of the high-frequency ν_{CO} mode varies over a very narrow range, upon going from the two basic ligands diethylamine **a** (pK_a = 10.84) and triethylamine **b** (pK_a = 10.75) to the less basic imidazole **c** (pK_a = 6.95) and 1-methylimidazole **d** (pK_a = 7.13). With less basic pyrazole **e** (pK_a = 2.09), 1-methylpyrazole **f** (pK_a = 2.52), and 3,5-dimethylpyrazole **g** (pK_a = 4.12) ligands, this value shifts in a magnitude of ca. 5 cm^{-1} toward higher frequency.[14] The difference of 73–79 cm^{-1} between the two carbonyl stretching frequencies is large and therefore consistent with a significant coupling between the two CO vibrators.[15] It is well established that the carbonyl stretching frequency can be used as an indicator of the electronic density on the metal center.[16] Indeed, evaluation of the average frequency for the two CO stretching modes of **3** demonstrates that the electronic density provided to the rhodium center by the ligand follows the order **b** > **a** ≈ **d** > **c** > **g** > **f** ≈ **h** > **e**.

X-ray crystal structures of **3a** and **3d**–**3f** were resolved, and the molecular view of **3a** and the packing diagram of **3f** are displayed in Figures 1 and 2, respectively. Relevant bond length and angle parameters are listed in Table 2. The data for **3d** and **3e** are in very good agreement with those reported previously by Oro et al.[11b] and Stobbart et al.[12c] (see the Supporting Information, SI). In all cases, the C2–Rh1–C1 angle is ~90°. The longest Rh1–N1 bond distance is 2.124(2) Å for **3a**, which is consistent with the absence of retrodonation of the very basic aliphatic diethylamine ligand.

Unlike the previously characterized chloro analogues **3d**[11b] and **3e**[12c] or $[RhCl(CO)_2(NH_2R)]$[10b] (R = linear alkyl group), there are no molecular wires through intermolecular Rh–Rh interactions for **3a** and **3f**, presumably because of the steric hindrance. Indeed, in **3a**, the two ethyl substituents are located above and below the rhodium coordination plane, and in **3f**, ligand **f** is almost perpendicular to the coordination plane,

dx.doi.org/10.1021/ic2019988 | Inorg. Chem. 2012, 51, 8670–8685

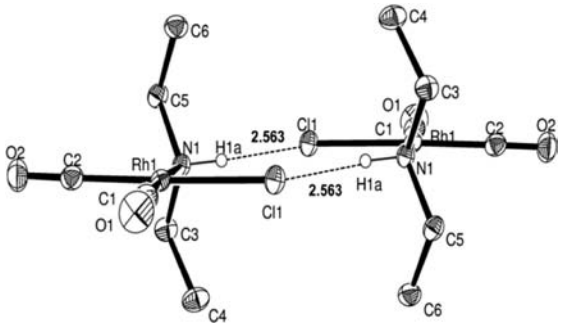

Figure 1. Molecular view putting in evidence the intermolecular hydrogen-bonding interaction (2.563 Å) between two molecules of **3a**. Thermal ellipsoids are shown at the 30% probability level, and hydrogen atoms are omitted for clarity, except for the amine group involved in the intermolecular hydrogen bond.

which results in a significantly longer Rh−Rh distance (3.237 and 3.392 Å for **3d** and **3e** vs 7.475 and 13.092 Å for **3a** and **3f**, respectively).

For **3a**, an intramolecular N1−H1a···Cl1 distance (2.722 Å) is within the range expected for a hydrogen-bonding interaction (2.20−3.25 Å).[17] However, the relatively small N1−H1···Cl1 angle (106.73°) is not consistent with the definition of a proper hydrogen-bonding interaction.[18] In contrast, the packing diagram of **3a** shows a N1−H1a···Cl1 intermolecular interaction, with corresponding distance and angle of 2.563 Å and 146.75°. respectively. Noteworthy for **3e**, the intramolecular N2−H2a···Cl1 distance and angle of 2.463 Å and 130.13°, respectively, are indicative of a hydrogen-bonding interaction involving N−H···Cl atoms, which was not mentioned in earlier studies.[11b,12c] The packing diagram of **3f** (Figure 2) shows an intermolecular C3−H···Cl1 distance of 2.815 Å and a C3−H···Cl1 angle of 138.73°.

The room temperature solution ^{1}H and $^{13}C\{^{1}H\}$ NMR data are consistent with the molecular X-ray structures described above. Complexes **3** were ^{13}CO-enriched prior to $^{13}C\{^{1}H\}$ NMR measurements. The $^{13}C\{^{1}H\}$ NMR spectra for **3a**, **3d**, **3f**, and **3g** feature a set of two doublets present in the carbonyl region as expected. However, the $^{13}C\{^{1}H\}$ NMR spectra for **3c**, **3e**, and **3h** display only a broad singlet or a doublet, which is indicative of fluxional behavior.[19] Chemical shift and coupling constant data for carbonyl ligands are shown in Table 3. The ^{1}J coupling constant between Rh and C1O1 in the trans position to the nitrogen-containing ligand is higher than that for *cis*-C2O2, which is consistent with the somewhat shorter C1−O1 bond length in comparison with C2−O2.

Table 2. Selected Bond Lengths (Å) and Angles (deg) for *cis*-3

atom	3a	3d	3e	3f
Rh1−N1	2.124(2)	2.096(2)	2.089(1)	2.094(2)
Rh1−Cl1	2.340(1)	2.374(1)	2.365(1)	2.333(1)
Rh1−C1	1.857(2)	1.857(4)	1.847(2)	1.844(2)
Rh1−C2	1.839(2)	1.843(4)	1.851(2)	1.847(2)
C1−O1	1.132(2)	1.127(4)	1.130(2)	1.131(2)
C2−O2	1.134(2)	1.134(4)	1.130(2)	1.132(3)
N1−H1a···Cl1 intra[b]	2.722			
N2−H2a···Cl1 intra[b]			2.463	
Rh···Rh inter (along the *b* axis)	7.475	3.237[a]	3.392[a]	13.092
N1−H1a···Cl1 inter[c]	2.563			
C4−H···Cl1 inter[c]		2.830	2.877	
C3−H···Cl1 inter[c]				2.815
C2−Rh1−C1	91.20(9)	89.67(13)	90.08(7)	89.83(9)

[a]Stacking arrangement along the *b* axis. [b]Intramolecular H···Cl distance. [c]Shortest intermolecular H···Cl distance.

Synthesis and Characterization of Iodorhodium(I) Complexes [RhI(CO)$_2$(L)] (4). Starting from the iodo-bridged $[Rh(\mu\text{-}I)(CO)_2]_2$ complex precursor **2**, the rhodium(I) complexes *cis*-**4a**−**4h** were prepared in the same manner as the chloro analogues **3** (Scheme 1). Because the iodo complexes are usually more air- and moisture-sensitive and/or thermally sensitive, the synthesis of **4** was carried out at temperatures ranging from 263 K to room temperature. Complexes **4a** and **4c**−**4h** were fully characterized by FT-IR and conventional NMR spectroscopies, mass spectrometry, elemental analyses, and single-crystal X-ray crystallography. Complex **4b** was only characterized in situ by FT-IR because attempts to isolate it were unsuccessful. IR data of the characteristic ν_{CO} stretching frequencies of **4** in CH_2Cl_2 are displayed in Table 4.

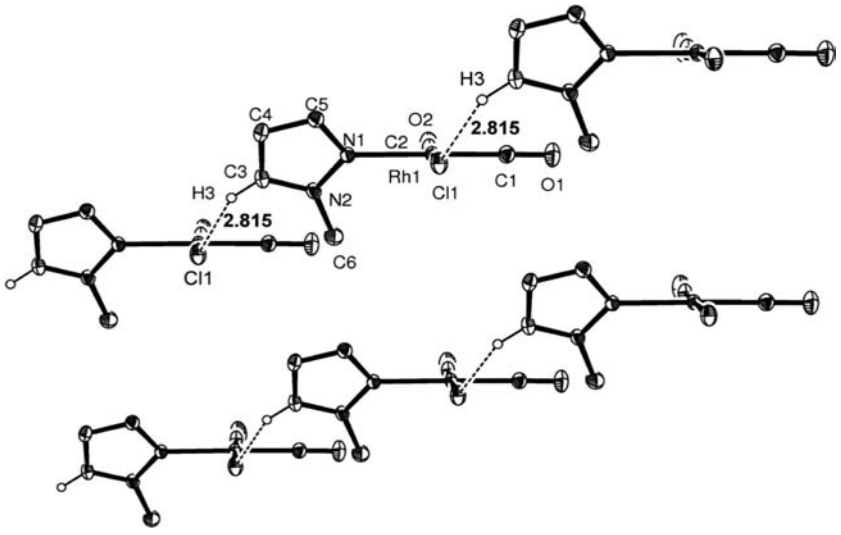

Figure 2. Packing diagram of **3f**. Thermal ellipsoids are shown at the 30% probability level, and hydrogen atoms are omitted for clarity, except for the carbon atom involved in an intermolecular hydrogen-bonding interaction (2.815 Å).

dx.doi.org/10.1021/ic2019988 | *Inorg. Chem.* 2012, 51, 8670−8685

Table 3. $^{13}C\{^1H\}$ NMR Data for *cis*-3[a]

	$\delta_{^{13}CO}$, ppm		$^1J_{CO-Rh}$, Hz	
complex	*cis*-C2O	*trans*-C1O	*cis*-C2O	*trans*-C1O
3a	183.5 (d)	181.2 (d)	65.7	75.5
3c	183.04 (br)			
3d	184.4 (d)	181.2 (d)	64.5	73.9
3e	182.1 (d)		70.8	
3f	183.3 (br d)	180.0 (br d)	~51.4	~60.1
3g	183.8 (d)	180.6 (d)	62.0	80.2
3h	180.55 (d)		67.9	

[a]NMR solvent = CD_2Cl_2; 298 K; C1O in the trans position with respect to the nitrogen ligands; $^2J_{C-C}$ coupling is very small and therefore not detected.

Table 4. IR Carbonyl Stretching Frequencies for *cis*-4

	IR (CH_2Cl_2)		
complex	ν_{CO}, cm^{-1}	$\Delta\nu_{CO}$, cm^{-1}	$\nu_{av(CO)}$, cm^{-1}
4a	2077.6, 2005.8	71.8	2041.7
4b	2076.4, 2003.5	72.9	2040.0
4c	2077.9, 2008.1	69.8	2043.0
4d	2077.0, 2007.1	69.9	2042.1
4e	2082.4, 2015.0	67.4	2048.7
4f	2082.0, 2013.4	68.6	2047.7
4g	2080.2, 2011.9	68.3	2046.1
4h	2081.3, 2013.4	67.9	2047.4

As observed above for **3**, two bands of similar intensity are observed in the carbonyl region, illustrating the square-planar configuration with two CO ligands in mutual cis positions.

The high-frequency ν_{CO} bands for complexes **4** appear at ca. 7 cm^{-1} lower frequency than those for the corresponding chloro complexes **3** because of the stronger back-donation induced by the iodo ligand. Analysis of these ν_{CO} values generally shows a correlation with the ligand basicity. Ligands **a**–**d** of similar basicity exert almost the same electronic influence, while the less basic **e**–**g** ligands increase the ν_{CO} values by ca. 5–6 cm^{-1} (Tables 1 and 4). The diethylsulfide ligand **h** shows electronic behavior similar to that of **e**–**g**. The electron density provided to the rhodium center by the ligand follows an order similar to that determined for the chloro analogues **3**: **b** > **a** ≈ **d** > **c** > **g** > **f** ≈ **h** > **e**.

The X-ray ORTEP diagrams of complexes **4a** and **4d**–**4f** are depicted in Figures 3–6. Relevant bond lengths and angles are listed in Table 5. The Rh1–C1 and C1–O1 distances for CO trans to the ligand L are similar for both chloro and iodo complexes.[20] A similar comparison prevails for the Rh1–C2 bond distances.

For complexes **4d** and **4e**, the molecular packing diagrams dominantly adopt the stacking of square-planar rhodium units along the *b* axis, which result in slightly zigzag wires of rhodium atoms with Rh···Rh···Rh angles of 153.5° and 157.6°. The Rh···Rh metal distances are 3.875 and 3.599 Å, respectively. This shorter Rh···Rh intermolecular distance for **4e** is consistent with the smaller angle formed by the rhodium coordination plane with the N-heterocyclic ring (7.7° for **4e** vs 35.1° for **4d**). Such 1D molecular chains formed via Rh···Rh interaction are also observed for chloro analogues **3d**[11b] and **3e**[12c] (see the SI) and other d^8 rhodium(I) complexes.[9a,b,21] The separated wires of stacked units are staggered along the *c* axis, resulting in a Rh···Rh distance of 7.246 Å for **4d** and 7.540 Å for **4e**. For **4f**, the 1-methylpyrazole ring is almost perpendicular to the coordination plane (87.1°), so that the intermolecular Rh···Rh distance is much longer (9.374 Å).

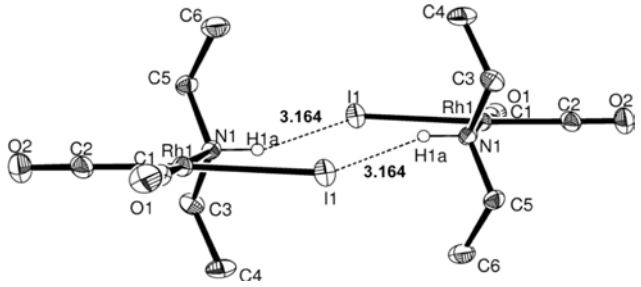

Figure 3. Molecular view putting in evidence the intermolecular hydrogen-bonding interaction (3.164 Å) between two molecules of **4a**. Thermal ellipsoids are shown at the 30% probability level, and hydrogen atoms are omitted for clarity, except for the amine group involved in the intermolecular hydrogen bond.

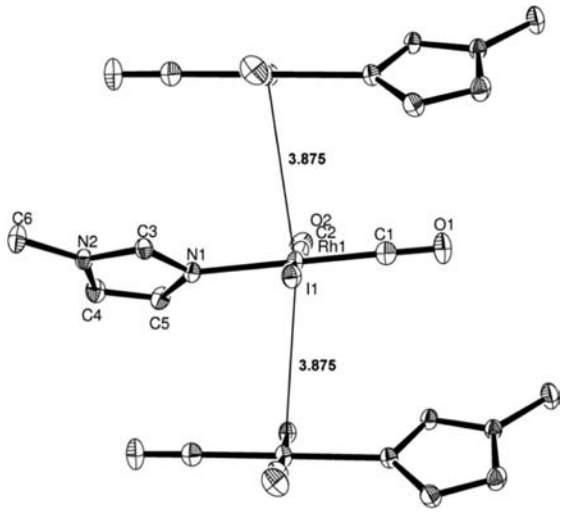

Figure 4. Packing arrangement of **4d** stacked parallel to the *b* axis. Thermal ellipsoids are shown at the 30% probability level, and hydrogen atoms are omitted for clarity.

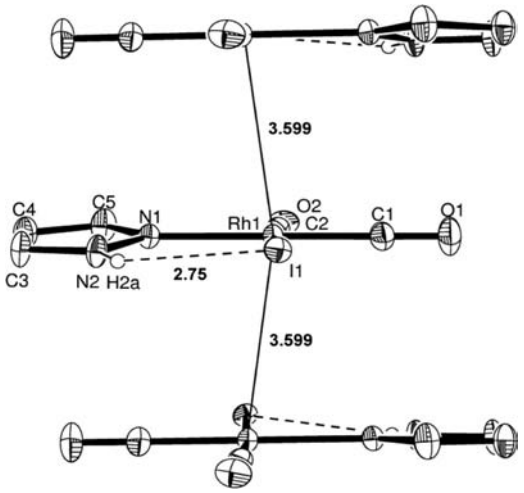

Figure 5. Packing arrangement of **4e** stacked parallel to the *b* axis. Thermal ellipsoids are shown at the 30% probability level, and hydrogen atoms are omitted for clarity, except for the amine group involved in an intramolecular hydrogen-bonding interaction (2.75 Å).

dx.doi.org/10.1021/ic2019988 | Inorg. Chem. 2012, 51, 8670–8685

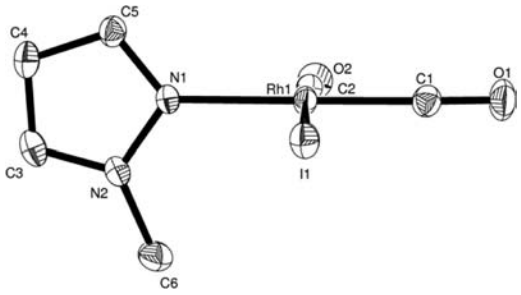

Figure 6. Representation of one molecule of **4f** from the asymmetric unit. Thermal ellipsoids are shown at the 30% probability level, and hydrogen atoms are omitted for clarity.

An intramolecular hydrogen-bonding interaction has been detected for **4e**: The N1−H1a···I1 distance and angle are 2.750 Å and 134.36°, respectively.[22] In addition, the packing configurations lay out several different intermolecular hydrogen-bonding interactions for **4a** and **4d**−**4e**. For **4a**, the N1−H1a···I1 contact distance is 3.164 Å and the corresponding angle is 127.85°;[23] for **4d** and **4e**, the C4−H4···I1 contact distances are 3.214 and 3.223 Å with corresponding angles of 146.92° and 144.48°, respectively (Figures 4−6). In fact, for **3a**, **3d**, **3e**, **4a**, **4d**, and**4e**, the observation of multiple CO bands on the attenuated total reflectance infrared (ATR-IR) spectra indicates the reduced symmetry for the $[Rh(CO)_2]$ moieties, presumably because of the presence of strong intra- and/or intermolecular interactions.[10f] By contrast, for **3f** and **4f**, two neat ν_{CO} bands of almost the same intensity are observed, which reflect the absence of weak intra- and/or intermolecular interactions (see the SI).

Variable-Temperature NMR (VT-NMR) Studies of Complexes 4. Complexes **4a** and **4c**−**4h** have been characterized by ^1H and $^{13}C\{^1H\}$ NMR. Like complexes **3**, complexes **4** were ^{13}CO-enriched prior to $^{13}C\{^1H\}$ NMR analyses. At room temperature, the $^{13}C\{^1H\}$ NMR spectrum of **4a** in the carbonyl region features two doublet of doublets, whereas two larger ones are observed for **4c** and **4d**, which correspond to the two CO in mutual cis positions. The ^1H NMR spectrum of **4a** consists of two sets of broad multiplets centered at 2.97 and 3.07 ppm in a 1:1 ratio for the methylene protons on the ethyl substituents of **a**, while in the case of **3a**, only one broad multiplet centered at 3.02 ppm is observed. This indicates that in both cases the two CH_2 groups are diastereotopic, as previously reported for $[RhCl(CO)(PPh_3)(\mathbf{a})]$.[17a] In contrast, $^{13}C\{^1H\}$ NMR spectra of **4e**−**4h** recorded at room temperature exhibit only one broad singlet, which is indicative of a fluxional behavior. Therefore, ^1H and $^{13}C\{^1H\}$ VT-NMR experiments have been performed for **4c**−**4h**. Selected chemical shifts and coupling constants are displayed in Table 6.

The rapid dynamic site exchange of the coordinated ligands **e**−**h** on the NMR time scale gives rise to a time-averaged carbonyl chemical shift at room temperature, as observed previously for **3f**.[19] At low temperature, the exchange rate is slowed down, and broad signals split into two sharp doublet of doublets, which is indicative of a static structure in solution. Figure 7 displays a series of $^{13}C\{^1H\}$ VT-NMR spectra for **4f** in the carbonyl region at 203−298 K.

In parallel to the ligand-exchange phenomenon, in the case of **4e** and **4g**, a simultaneous hydrogen exchange from one nitrogen atom to the other occurs. A set of ^1H NMR spectra for **4e** at temperatures ranging from 223 to 303 K are depicted in Figure 8. At 303 K, a broad time-averaged signal at 7.78 ppm is assigned to the two H_a and H_b proton atoms in close vicinity to the N1 and N2 atoms of the pyrazole ring, which indicates a fast hydrogen-exchange process on the NMR time scale. This signal then splits into two pseudotriplets when the temperature is decreased.[24]

Coalescence temperatures (T_c) and activation parameters ($\Delta H^{\ddagger}$, $\Delta S^{\ddagger}$, and E_a) for **4** have been determined and are listed in Table 7 (see the SI). The activation enthalpy $\Delta H^{\ddagger}$ is generally related to the lability of the ligands and therefore to their electronic and steric contributions.[19c] The significantly lower T_c values for **4e**−**4g** in comparison with those for **4c** and **4d**[25] indicate a higher labile character (faster ligand exchange) of pyrazole-type ligands, which is consistent with their lower electron-donating ability (higher $\nu_{av(CO)}$ values). In all cases, the obtained negative values of $\Delta S^{\ddagger}$ suggest that an associative ligand-exchange mechanism is operative. Substitution of a hydrogen atom by methyl groups on the N2 atom (ligand **f**) or on C3−C5 atoms (ligand **g**) of the pyrazole ring results in an insignificant variation of E_a values. The lowest estimated

Table 5. Selected Bond Lengths (Å) and Angles (deg) for *cis*-4

				4f[d]	
atom	4a	4d	4e	Mol1	Mol2
Rh1−N1	2.134(3)	2.102(2)	2.099(2)	2.099(3)	2.099(3)
Rh1−I1	2.645(1)	2.660(1)	2.662(1)	2.660(1)	2.660(1)
Rh1−C1	1.862(5)	1.844(3)	1.838(3)	1.839(5)	1.841(4)
Rh1−C2	1.857(4)	1.863(3)	1.862(3)	1.855(4)	1.847(5)
C1−O1	1.128(5)	1.138(3)	1.133(4)	1.135(5)	1.133(5)
C2−O2	1.120(5)	1.127(3)	1.134(3)	1.125(5)	1.140(5)
N1−H1a···I intra[b]	2.898				
N2−H2a···I intra[b]			2.750		
Rh···Rh (along the *b* axis)	12.626	3.875[a]	3.599[a]	9.374	9.374
Rh···Rh (along the *c* axis)	4.884	7.246	7.540		
N1−H1a···I inter[c]	3.164				
C1−Rh1−C2	91.30(19)	90.67(12)	89.65(13)	90.22(18)	90.73(18)
Rh···Rh···Rh (zigzag stacking)		153.5	157.6		
I−Rh−$(CO)_2$ plane/nitrogen ligand		35.1	7.7	86.9	76.9

[a]Stacking arrangement along the *b* axis. [b]Intramolecular H···I distance. [c]Shortest intermolecular H···I distance. [d]The crystal cell contains two molecules (Mol1 and Mol2).

dx.doi.org/10.1021/ic2019988 | *Inorg. Chem.* 2012, 51, 8670−8685

Table 6. $^{13}C\{^1H\}$ VT-NMR Data for *cis*-4[a]

		$\delta_{^{13}CO}$, ppm		$^1J_{CO-Rh}$, Hz		
complex	*T*, K	*cis*-C2O	*trans*-C1O	*cis*-C2O	*trans*-C1O	$^2J_{CO-CO}$, Hz
4a	298	184.5 (dd)	180.2 (dd)	65.4	79.5	4.1
4c[b]	298	185.7 (br d)	180.0 (br d)	63.2	70.8	
	233	186.1 (d)	179.9 (d)	61.9	76.5	
4d	298	185.0 (br d)	180.1 (br d)		73.0	
	243	185.4 (d)	179.8 (d)	62.4	77.9	
4e	298	181.6 (br s)				
	223	184.9 (d)	179.1 (d)	62.9	78.0	4.4
4f	298	182.0 (br s)				
	203	185.2 (d)	178.9 (d)	59.1	75.5	4.8
4g	298	181.3 (br s)				
	193	184.6 (d)	178.2 (d)	62.9	78.0	
4h	298	180.8 (br s)				
	183	182.5 (d)	180.1	66.7	76.8	

[a]NMR solvent = CD_2Cl_2. [b]CD_3OD; C1O in the trans position with respect to the ligands **a**–**h**.

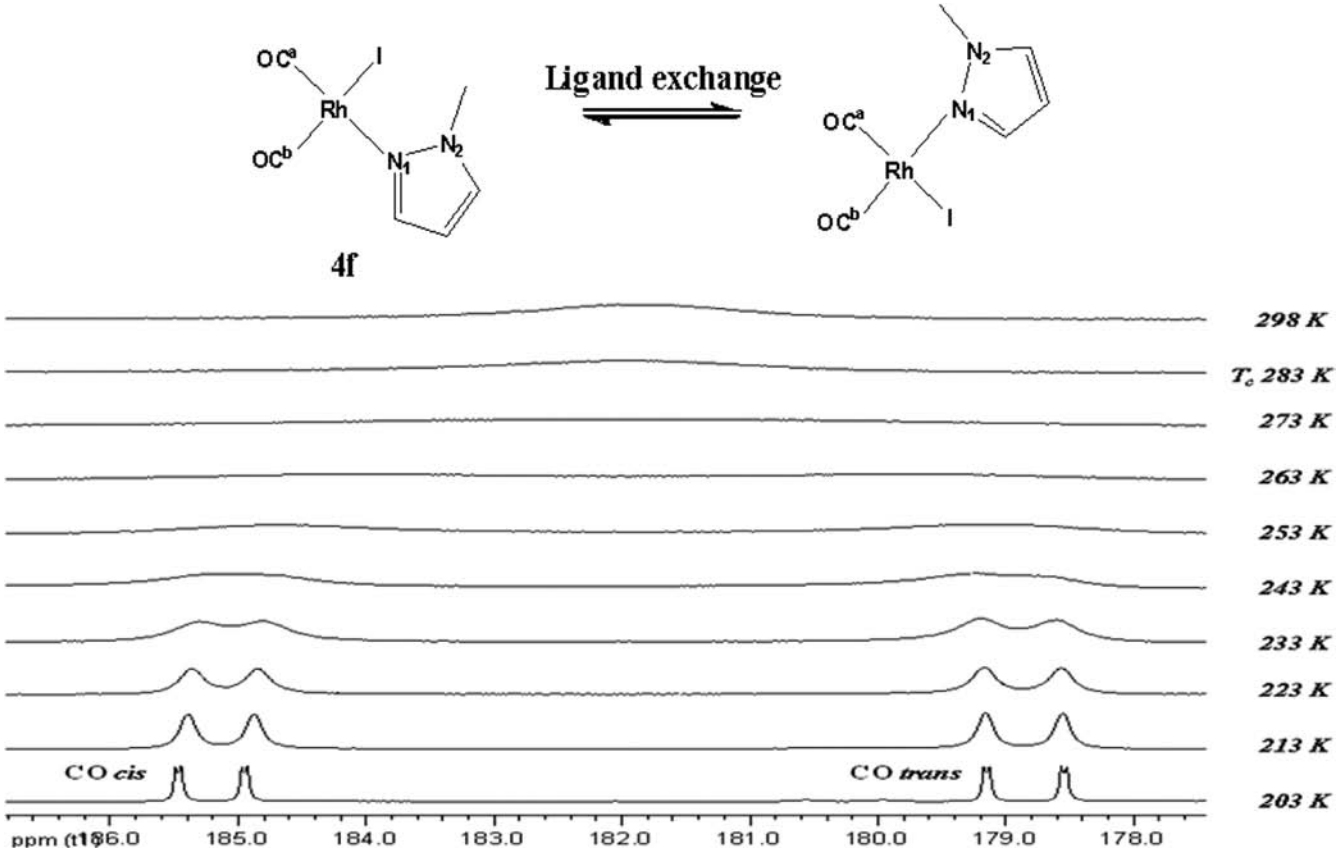

Figure 7. $^{13}C\{^1H\}$ VT-NMR stacking spectra in the carbonyl region of 4f at 203–298 K in CD_2Cl_2.

Arrhenius activation energy E_a is 16.21 kJ mol^{-1} (T_c = 223 K) for **4h**, which reflects the high labile character of SEt_2 compared to the amine derivatives.[26] It is worth noting that for **4e** the lower hydrogen-exchange E_a value in comparison with the ligand-exchange E_a value, with a negative $\Delta S^{\ddagger}$ value, probably involves an associative hydrogen-exchange mechanism.

In addition, ^{15}N chemical shifts for **4d**–**4f** have been determined throughout 2D $^1H-^{15}N$ HMBC NMR experiments. For **4d** at 298 K, a broad doublet that resonates at −189.8 ppm with a $^1J_{N-Rh}$ of 23.5 Hz is assigned to the nonsubstituted N1 atom and a broad signal that appears at −214.2 ppm is assigned to the methyl-substituted nitrogen atom N2. In the same manner, ^{15}N chemical shifts corresponding to the Rh–N1 and N2 atoms for **4e** and **4f** were determined at −158.7 and −171.3 ppm (250 K) and −153.9 and −178.6 ppm (298 K), respectively.[27] Furthermore, ($^1H-^{103}Rh$) 2D HMQC NMR measurements carried out at 243 K for **4e** and **4f** present characteristic rhodium(I) signals at − 8387 and −8334 ppm, respectively.[28]

Synthesis and Characterization of Acetylrhodium(III) Complexes. CH_3I addition reactions toward complexes **4a** and **4c**–**4h** have been evaluated. Indeed, the reaction of **4c**–**4g** with neat CH_3I affords the corresponding neutral dimeric iodo-bridged acetylrhodium(III) complexes $[RhI(\mu\text{-}I)(COMe)(CO)(L)]_2$ (**6c**–**6g**; L = **c**–**g**) in high isolated yields.

dx.doi.org/10.1021/ic2019988 | *Inorg. Chem.* 2012, 51, 8670–8685

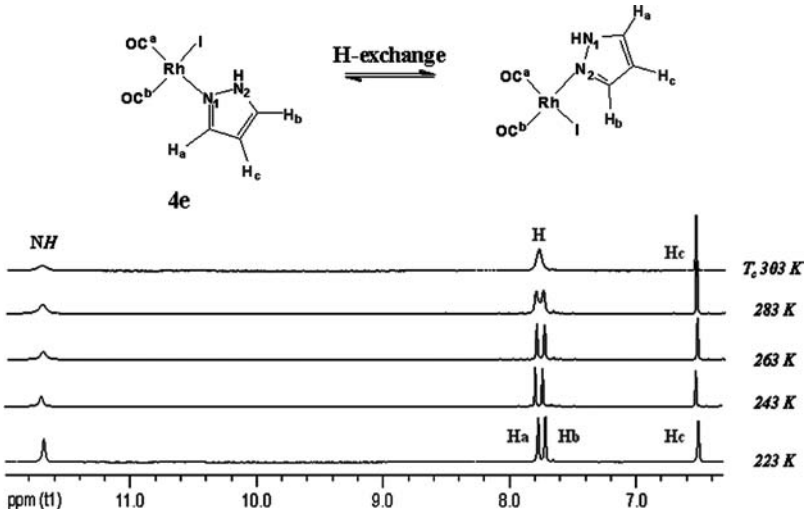

Figure 8. ^{1}H VT-NMR stacking spectra of **4e** at 223−303 K in CD_2Cl_2.

Table 7. Coalescence Temperature T_c and Activation Parameters for *cis*-4[a]

complex	T_c, K	E_a, kJ mol^{-1}	$\Delta H^{\ddagger}$, kJ mol^{-1}	$\Delta S^{\ddagger}$, J K^{-1} mol^{-1}
4a	≫328			
4c[b]	>328	26.9 ± 1.6	24.7 ± 1.5	−117 ± 7.0
4d	>295	29.0 ± 1.7	26.8 ± 1.6	−107 ± 6.4
4d[b]	328	26.7 ± 1.6	24.5 ± 1.5	−111 ± 6.7
4e	283	32.4 ± 1.9	30.2 ± 1.8	−76 ± 4.6
4e[c]	303	21.3 ± 1.3	19.0 ± 1.1	−141 ± 8.5
4f	283	32.7 ± 2.0	30.5 ± 1.8	−75 ± 4.5
4g	273	28.3 ± 1.7	26.1 ± 1.6	−89 ± 5.3
4h	223	16.2 ± 1.0	14.5 ± 0.9	−123 ± 7.4

[a]NMR solvent = CD_2Cl_2. [b]CD_3OD. Ligand-exchange process. [c]Hydrogen-exchange process. T_c = coalescence temperature.

Under analogous conditions, **4a** mainly gives a mixture of neutral $[RhI(\mu\text{-}I)(COMe)(CO)(\mathbf{a})]_2$ (**6a**) and ionic $[RhI_2(\mu\text{-}I)(COMe)(CO)]_2[HNMeEt_2]_2$, whereas **4h** exclusively produces ionic $[RhI_2(\mu\text{-}I)(COMe)(CO)]_2[SMeEt_2]_2$ as the final compound. In parallel, **6c−6h** were prepared according to a method developed by Haynes et al.[29] in a two-step reaction: **2** is treated at room temperature with CH_3I in acetonitrile to produce the stable dimeric complex $[RhI(\mu\text{-}I)(COMe)(CO)(CH_3CN)]_2$ (**5**), which is further substituted with 2 mol equiv of ligands **c−h** (Scheme 2).[30]

Relevant FT-IR data of **6−8** in CH_2Cl_2 and neat CH_3I are summarized in Table 8. FT-IR spectra of the dimeric rhodium(III) **6** show a broad and intense terminal ν_{CO} band at ∼2070 cm^{-1}, i.e., 35 cm^{-1} higher in frequency than the $\nu_{av(CO)}$ value of the starting complexes **4**, which is consistent with a rhodium(III) carbonyl fragment. In addition, a broad medium ν_{COMe} acetyl band appears at ∼1700 cm^{-1}.

The ^{1}H and $^{13}C\{^1H\}$ NMR spectra for **6** clearly identify the acetyl group with a proton signal at ∼3.0 ppm and a methyl carbon signal at ∼48.0 ppm, respectively. The $^{13}C\{^1H\}$ NMR

Table 8. IR Carbonyl Stretching Frequencies for 6−8 at Room Temperature

	CH_2Cl_2		CH_3I	
complex	ν_{CO}, cm^{-1}	ν_{COMe}, cm^{-1}	ν_{CO}, cm^{-1}	ν_{COMe}, cm^{-1}
6a	2072.6	1719.1	2063.3	1716.4
6c	2073.7	1734.9, 1707.0	2073.9	1719.2, 1705.2
6d	2073.1	1733.5	2068.0	1736.0
6e	2083.5	1741.0, 1721.0	2075.6	1736.7
6f	2076.6	1778.0	2072.3	1776.4, 1743.7
6g	2079.6	1753.8	2075.5	1749.6
6h	2080.6	1720.8	2076.4	1743.6
7d[a]	2073.2	1735.9		
8e	2082.5	1698.9, 1677.4		

[a]A very weak symmetric band has been observed at 2155.6 cm^{-1}.

Scheme 2. General Reaction Pathway Leading to the Acetylrhodium(III) Complexes 5−8

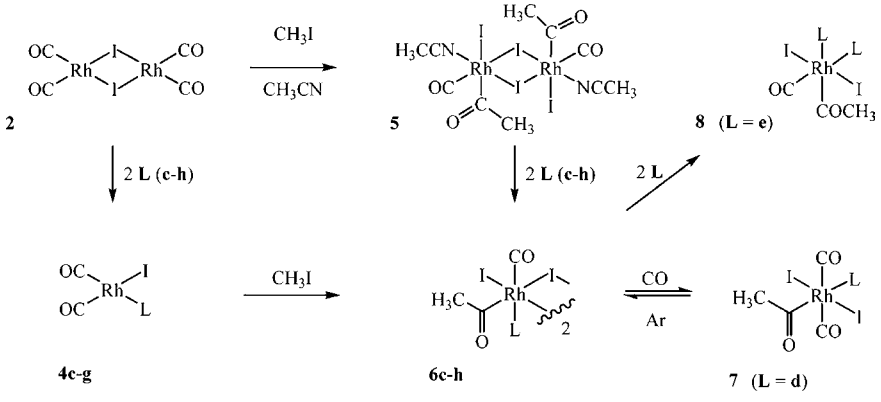

dx.doi.org/10.1021/ic2019988 | Inorg. Chem. 2012, 51, 8670−8685

spectra in the carbonyl region for **6** exhibit a group of signals centered at ~212 ppm, which was assigned to Rh−$COCH_3$, and another group centered at a higher field of ~182 ppm, which is attributed to the terminal Rh−*C*O. The broad carbonyl IR bands and ^{13}CO NMR pattern (multiplicity) of doublet observed at room temperature for **6** indicate the existence of several isomers in solution, which is consistent with the previous results reported on an iodo-bridged rhodium dimer.[31] Even at low temperature (193 K), $^{13}C\{^1H\}$ NMR spectra of *cis*-[RhI(μ-I)(COMe)(CO)(**e**)]$_2$ (**6e**) still display very broad signals.[32]

The reactivities of complexes **6d** and **6e** toward CO and an extra nitrogen-containing ligand **e** have been explored. Brief CO bubbling (10 min) of a dichloromethane solution containing **6d** results in the sharpening of both characteristic IR bands (ν_{CO} and ν_{COMe}) and the corresponding $^{13}C\{^1H\}$ NMR signals [δ_{COMe} = 210.2 (d) ppm, $^1J_{COMe-Rh}$ = 21.6 Hz; δ_{CO} = 183.4 (d) ppm, $^1J_{CO-Rh}$ = 58.5 Hz). These data are consistent with the formation of the monomeric complex [RhI_2(COMe)-$(CO)_2$(**d**)] (**7d**), which has a much lower number of isomers in solution (Scheme 2). In the absence of a CO atmosphere, **7d** loses gradually one CO to form the initial dimeric **6d** species, as was previously observed for the anionic complex [RhI_3-(COMe)$(CO)_2]^-$ (see the SI).[31] Furthermore, keeping the solution of **7d** in dichloromethane under a CO atmosphere for a longer period of time (48 h) affords the starting rhodium(I) species **4d**.[33]

The treatment of **6e** with 2 equiv of ligand **e** quantitatively yields the monomer [RhI_2(COMe)(CO)(**e**)$_2$] (**8e**) bearing two pyrazole ligands in the coordination sphere (Scheme 2). In the FT-IR spectrum, the terminal ν_{CO} band at 2082.5 cm^{-1} shifts only slightly by 1 cm^{-1}, whereas the acetyl bands (1698.9 and 1677.4 cm^{-1}) shift drastically by more than 40 cm^{-1} to lower wavenumber with respect to the initial dimeric complex **6e**, which suggests that **e** is coordinated in the trans position to the acetyl ligand. Complete ^1H and ^{13}C NMR chemical shift assignments for two distinctly bound pyrazole ligands have been determined from the interpretation of 2D $^1H-^1H$ COSY and $^1H-^{13}C$ HMQC NMR experiments (see the SI). A broad time-averaged ^1H signal at room temperature for both C3−*H* and C5−*H* of one pyrazole ring is observed, which agrees with the fluxional hydrogen-exchange process described earlier. In contrast, for the other ring, the observation of two well-separated ^1H signals suggests that N−*H* remains static on the NMR time scale.

Suitable single crystals for X-ray analysis of the isomer *trans*-[RhI(μ-I)(COMe)(CO)(**d**)]$_2$ (**6d$_1$**) and **6e** were grown in CH_2Cl_2 at 255 K, and their molecular views are displayed in Figures 9 and 11. Attempts for crystallization of **7d** in CH_2Cl_2 gave another unexpected isomer *cis*-[RhI(μ-I)(COMe)(CO)-(**d**)]$_2$ (**6d$_2$**; Figure 10). Selected bonds and angles are listed in Tables 9 and 10. The molecular structure of **6d$_1$** is centrosymmetric, similar to that of [RhI_2(COMe)(CO)(L)][29] (L = NCMe, NC^{t}Bu) and [RhI_3(COMe)$(CO)]_2^{2-}$,[34] whereas **6d$_2$** and **6e** possess two apical terminal CO ligands in mutual cis positions as well as two apical ligands **d** and **e**. In all cases, the two acetyl moieties are located in the equatorial plane mutually trans to each other. The same arrangement prevails for the terminal iodo ligands, which afford a local centrosymmetric structure for the {$Rh_2(\mu$-I)$_2I_2(COCH_3)_2$} framework. The Rh1−I3 bond length (2.96−3.00 Å) is much longer than the two mutually trans I1−Rh1−I2 bonds (2.65−2.68 Å), indicating a large trans influence of the acetyl ligand. The

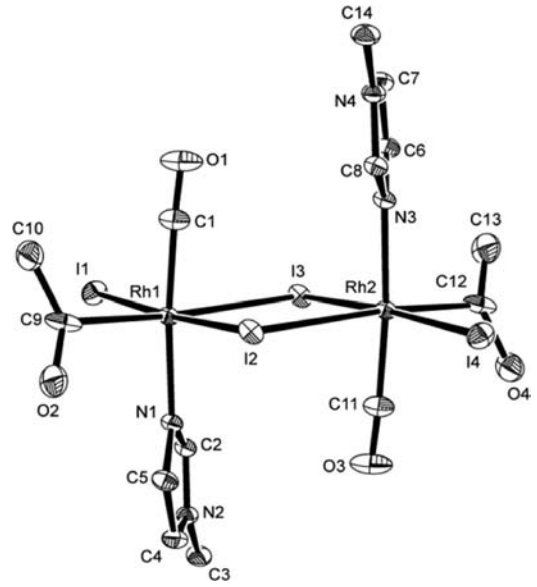

Figure 9. Molecular structure of the dimer **6d$_1$** from the asymmetric unit with an atom-labeling scheme. Thermal ellipsoids are shown at the 30% probability level, and hydrogen atoms are omitted for clarity.

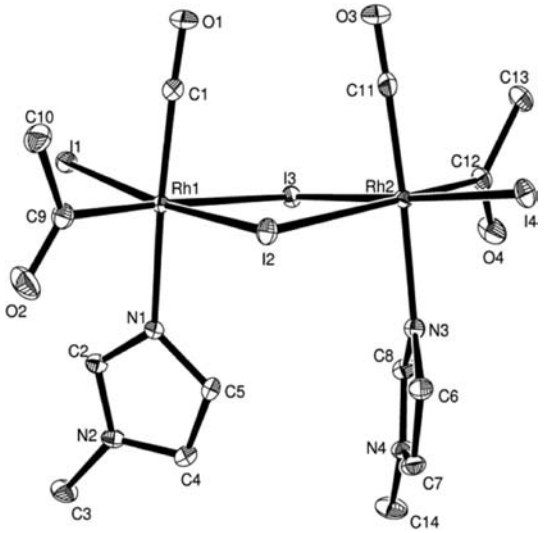

Figure 10. Molecular structure of the dimer **6d$_2$** with an atom-labeling scheme. Thermal ellipsoids are shown at the 30% probability level, and hydrogen atoms are omitted for clarity.

nonbonded Rh1−Rh2 distance is shorter for the centrosymmetric complex **6d$_1$** (4.010 Å) than for **6d$_2$** (4.105 Å) and **6e** (4.092 Å), which is consistent with a steric hindrance between the two nitrogen ligands in the cis apical position. In fact, the angles formed between both heterocyclic rings are 67.4° and 71.4° for **6d$_2$** and **6e**, respectively, whereas for **6d$_1$**, they are almost parallel.

Further analysis of the packing diagram of **6e** shows the existence of both intra- and intermolecular hydrogen-bonding interactions: the two intramolecular N2−H2a···O2 and N4−H4a···O4 distances are 2.149 and 2.028 Å with corresponding angles of 127.9° and 136.1°, respectively.[35] The intermolecular N2−H2a···I4 distance is 2.980 Å with an angle of 129.4°.

The X-ray crystal structure of **8e** was also solved (Figure 12 and Tables 9 and 10). The two pyrazole ligands are in mutual cis positions with the terminal carbonyl and acetyl ligands in

dx.doi.org/10.1021/ic2019988 | *Inorg. Chem.* 2012, 51, 8670−8685

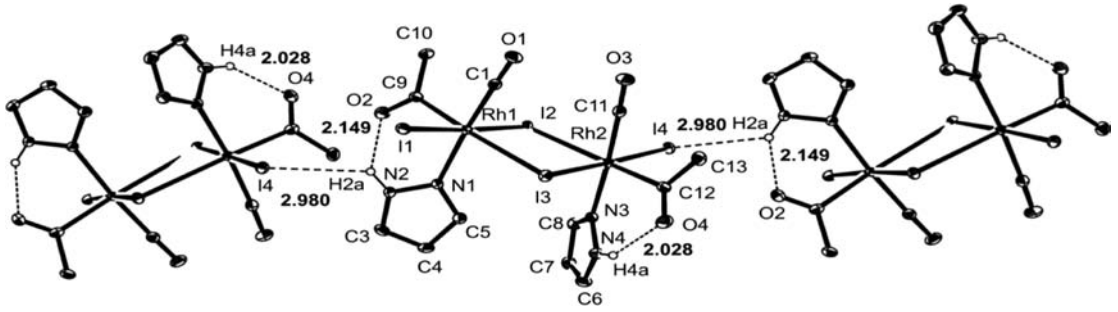

Figure 11. Molecular view of three molecules of dimer **6e**. Thermal ellipsoids are shown at the 30% probability level, and hydrogen atoms are omitted for clarity, except for the amine group, putting in evidence intramolecular (2.028 Å, 2.149 Å) and intermolecular (2.980 Å) hydrogen-bonding interactions.

Table 9. Selected Bond Lengths (Å) for $6d_1$, $6d_2$, 6e, and 8e

	$6d_1$[a]				
atoms	Mol1	Mol2	$6d_2$	6e	8e
Rh1−I1	2.653(1)	2.647(1)	2.662(1)	2.654(1)	2.674(1)
Rh1−I2	2.680(1)	2.669(1)	2.680(2)	2.671(1)	2.669(1)
Rh1−I3	2.958(1)	2.978(1)	2.960(2)	3.002(1)	
Rh1−C1	1.854(4)	1.859(5)	1.863(6)	1.856(3)	1.864(4)
Rh1−C9	2.217(6)	2.057(5)	2.037(6)	2.064(3)	2.042(4)
Rh1−N1	2.100(3)	2.105(3)	2.106(4)	2.104(3)	2.245(3)
Rh1−N3					2.107(3)
Rh2−I2	2.958(1)	2.978(1)	3.067 (2)	2.956(1)	
Rh2−I3	2.680(1)	2.669(1)	2.680(2)	2.682(1)	
Rh2−I4	2.653(1)	2.647(1)	2.640(2)	2.647(1)	
Rh2−C11	1.854(4)	1.859(5)	1.860(6)	1.868(3)	
Rh2−C12	2.217(6)	2.057(5)	2.044(5)	2.088(3)	
Rh2−N3	2.100(3)	2.105(3)	2.101(5)	2.107(3)	
N2−H2A···O2 intra				2.149	
N2−H2A···O2 inter					2.269
N4−H4A···O4 intra				2.028	
N4−H4A···O2 intra					2.082
Rh1···Rh2 intra	4.010	4.074	4.105	4.092	

[a]The crystal cell contains two molecules (Mol1 and Mol2).

Table 10. Rate Constants $k_{313\ K}$ for the Overall CH_3I Oxidative Addition Reaction of 4a and 4c−4g to 6a and 6c−6g

entry	IR $\nu_{(CO)}$, cm^{-1}	$\nu_{av(CO)}$, cm^{-1}	$k_{313\ K} \times 10^{-5}$, s^{-1}
4c	2073.3; 2002.8	2038.1	11.2
4d[a]	2072.4; 2002.0	2037.2	11.3
4e	2078.0; 2010.3	2044.2	1.3
4f	2077.6; 2009.2	2043.4	0.8
4g	2075.6; 2007.1	2041.4	1.7

[a]Experiment performed at 308 K.

the same plane, which is consistent with the NMR observations. The two iodo ligands occupy the apical positions toward the equatorial plane formed by N1−Rh−N3. The pyrazole rings trans and cis to the acetyl moiety are inclined toward the equatorial rhodium plane by 57.5° and 29.6°, respectively. The longer Rh1−N1 bond distance (2.245 Å), in comparison with the Rh1−N3 bond (2.107 Å), is in good agreement with the strong trans influence of the acetyl ligand.

Deeper analysis of the X-ray structure shows that both N−H atoms of each pyrazole ligand are involved in intramolecular N4−H4a···O2 (2.082 Å and 128.1°) and intermolecular N2−H2a···O2 (2.269 Å and 143.3°) interactions[35] (Tables 9 and 10). Indeed, the intramolecular contact results in the formation of a six-membered ring (Rh^I−N3−N4−H4a···O2−C9), which brings the *cis*-pyrazole plane closer to the equatorial rhodium plane in comparison with the trans one (29.6° vs 57.5°). It is very likely that this six-membered cycle is maintained in solution, preventing the H4a-exchange process to occur, as observed by the ^1H NMR study.

IR Monitoring of the Oxidative Addition Reaction of CH_3I on 4a and 4c−4h. We were interested in investigating the electronic and steric effects of the nitrogen-containing ligands on the CH_3I oxidative addition reaction. Because at low CH_3I concentration the reaction proceeds extremely slowly, we decided to perform IR-monitored studies in neat CH_3I so that its concentration remains quasi constant along the experiments. The stacking FT-IR spectra registered overtime in the 2200−1600 cm^{-1} region generally describe the decay of the anti-symmetric ν_{CO} bands for **4c−4g** followed by the appearance of the ν_{COMe} bands for **6c−6g** (see the SI). Even under these conditions, the reactions were very slow. At room temperature, the reaction rates require several days to be completed. Thus, the CH_3I oxidative addition reactions were operated at 313 K to be able to determine the initial rate constants (Table 10). The pseudo-first-order rate constants were found from the plot

dx.doi.org/10.1021/ic2019988 | *Inorg. Chem.* 2012, 51, 8670−8685

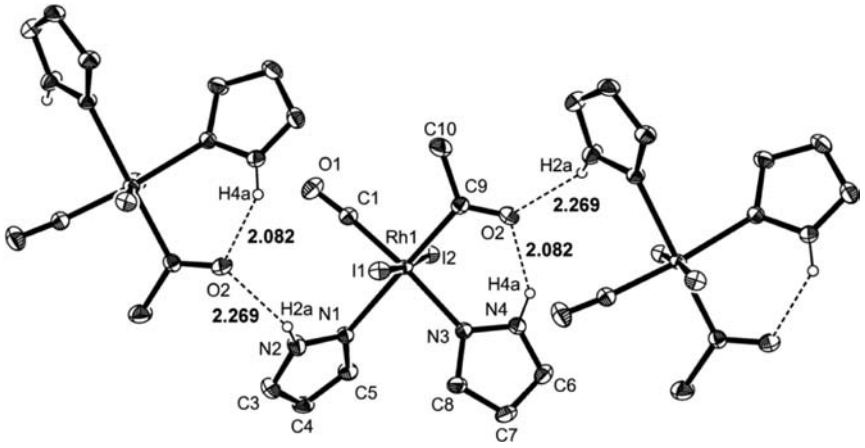

Figure 12. Molecular view of three molecules of **8e**. Thermal ellipsoids are shown at the 30% probability level, and hydrogen atoms are omitted for clarity, except for the amine group, putting in evidence intramolecular (2.082 Å) and intermolecular (2.269 Å) hydrogen-bonding interactions.

of $\ln(A_t)$ versus time, where A_t is the antisymmetric ν_{CO} absorbance of **4c**−**4g** at the time *t*.

The rhodium complexes bearing the imidazole ligands (**4c** and **4d**) are ca. 10 times more active than those containing pyrazole ligands (**4e**−**4g**), which is consistent with the higher $\nu_{av(CO)}$ values observed for the three latter ligands. Moreover, the reaction rate constant value $k_{308\ K}$ (11.2×10^{-5} s^{-1}) for **4d** determined at 308 K is quite similar to that for **4c** at higher temperature (313 K), suggesting that complex **4d** is somewhat more reactive than **4c**, according to the slightly lower $\nu_{av(CO)}$ value (ca. 1 cm^{-1}) of **4d**. Similarly, the higher nucleophilicity toward CH_3I of **4g** in comparison with those of **4e** and **4f** follows a similar order determined from the $\nu_{av(CO)}$ values, which suggests that the electronic influence is the main reaction driving force.

It is worth noting that **4e** is slightly more reactive than **4f** despite the slightly higher $\nu_{av(CO)}$ of **4e**. This observation can be explained by the steric effect exerted by the pyrazole ligands in the coordination sphere of the rhodium center. The oxidative addition of CH_3I to a square-planar complex is commonly accepted to proceed in two elemental steps: (i) nucleophilic attack by the rhodium center at the carbon to displace I^- and (ii) coordination of I^- to the five-coordinate cationic methylrhodium(III) intermediate to saturate the coordination sphere. On the other hand, as described above from X-ray structural analyses, 1-methylpyrazole ligand **f** adopts a conformation with its plane inclined significantly from the rhodium coordination plane (torsion angle of ca. 77°) compared to pyrazole **e** (with a corresponding torsion angle of 7.7°). In **4f**, the N-methyl substituent of **f** is thus placed on one side of the metal coordination plane. During the oxidative addition, the CH_3I molecule will preferentially approach the opposite less-hindered side. The S_N2-type step takes place to generate an initial cationic intermediate $[RhI(Me)(CO)_2(\mathbf{f})]^+$ in which the vacant axial trans coordination site is sterically congested by the axial N-methyl group, which therefore inhibits the further I^- approach to the rhodium center.[36]

In the case of **4a** and **4h**, the mechanistic pathway is quite different. Indeed, the decay of the band at ca. 2000 cm^{-1} showing a marked shift to low frequency in the later stages of the reaction and the observation of the ionic acetyl complexes $[RhI_2(\mu\text{-}I)(COMe)(CO)]_2^{2-}$ in the final solution are consistent with the formation of the ionic intermediate species $[Rh(CO)_2I_2]^-$ during the reaction. This anionic species results from the decoordination of diethylamine and diethylsulfide ligands, which are further methylated to form the corresponding counterions $[MeNHEt_2]^+$ and $[MeSEt_2]^+$, respectively. The situation is even more complicated for **4a** because the $[NH_2Et_2]^+$ cation and *N*,*N*-diethylacetamide were also identified by NMR monitoring. We suspect that at least two parallel pathways are operating involving presumably neutral/ionic rhodium(I) complexes for oxidative addition and neutral acetylrhodium(III) species for reductive elimination, leading to this acetamide formation.[37]

CONCLUSION

In summary, a series of mononuclear square-planar rhodium(I) chloro and iodo dicarbonyl neutral complexes bearing diethylamine, imidazole, and pyrazole derivatives have been synthesized. The iodorhodium(I) N-heterocyclic complexes show fluxional behavior. In the solid state, various intra- and intermolecular H···I interactions have been observed. The oxidative addition of CH_3I has been performed on the iodo complexes **4** to form (except for **4a** and **4h**) the corresponding neutral dimeric acetylrhodium(III) complexes **6**, among which two isomers were structurally determined. The iodo-bridged **6d** and **6e** were further split by the addition of either CO or **e**, affording the corresponding monomeric rhodium(III) complexes **7d** and **8e**, as confirmed by their X-ray structures. The different reactivities of **4c**−**4g** for the CH_3I oxidative addition are both attributed to the electronic and steric effects induced by the nitrogen-containing ligands. However, the presence of a hard or very labile ligand in the rhodium coordination sphere can induce a different mechanistic pathway in which the ligand is methylated, resulting in the formation of classical $[RhI_2(CO)_2]^-$ species.

EXPERIMENTAL SECTION

Instrumentation and Materials. FT-IR spectra were collected on a Perkin-Elmer Spectrum One FT spectrophotometer with a 0.1 mm cell equipped with CaF_2 windows and ATR-IR. All NMR spectral data were recorded on Bruker DPX 300 or Avance 300−500 spectrometers with tetramethylsilane as the external reference for ^1H and ^{13}C, $[Rh(acac)_3]$ for ^{103}Rh, and nitromethane for ^{15}N. Chemical shifts are reported in ppm, and coupling constants (*J*) are given in hertz. Spectral assignments were made by means of routine 1D and 2D NMR experiments when appropriate. Mass spectral analyses were performed on a TSQ 7000 Thermo Electron spectrometer equipped with electron impact (EI) and chemical ionization (DCI) sources.

dx.doi.org/10.1021/ic2019988 | *Inorg. Chem.* 2012, 51, 8670−8685

The major m/z peak was reported with the intensity as a percentage of the base peak in brackets. Elemental analyses were measured with a precision superior to 0.3% at the Microanalysis Service at the LCC in Toulouse, France. All reactions were carried out using standard Schlenk techniques under an atmosphere of dry argon or in an MBraun glovebox containing dry argon and less than 1 ppm of oxygen. All solvents used for experiments were obtained from a solvent purification system (MB SPS-800). CD_2Cl_2 was dried using activated molecular sieves. $RhCl_3 \cdot xH_2O$ salt was supplied by Johnson Matthey. The reagents were procured from Aldrich Chemicals, France. Amine ligands were dried and distilled over KOH and degassed prior to use. N-Heterocyclic compounds were used as received. Methyl iodide (Aldrich) was distilled over calcium hydride and stored in foil-wrapped Schlenk tubes under argon to prevent the formation of I_2. The starting rhodium precursors $[Rh(\mu\text{-}Cl)(CO)_2]_2$ (**1**)[38] and $[Rh(\mu\text{-}I)(CO)_2]_2$ (**2**)[39] were synthesized according to literature procedures.

^{13}CO-Labeling Procedure for 2. A dichloromethane solution (V = 25 mL) containing **2** (500 mg, 0.87 mmol) was stirred vigorously at room temperature under a ^{13}CO atmosphere for 20 min. The formation of labeled product **2-^{13}CO** was followed by FT-IR spectroscopy, and the complex was isolated by solvent removal under reduced pressure.

Synthesis of Neutral Complexes *cis*-[RhCl(CO)$_2$(L)] (3). To a dichloromethane solution (V = 25 mL) of **1** (500 mg, 1.28 mmol) under stirring was added via cannulation a solution of 2 mol equiv of ligand (**a**, **b**, **d**, **e**, or **f**) in dichloromethane (V = 5 mL). The reaction mixture was vigorously stirred at room temperature for 6 h. After solvent removal under vacuum (or evaporated under CO flux), compounds **3** obtained were washed with cold pentane, dried under vacuum, and stored under argon at 255 K prior to use.

*Chloro(dicarbonyl)(diethylamine)rhodium(I) Complex [RhCl(CO)$_2$(HN(CH$_2$CH$_3$)$_2$)] (**3a**).* Light-orange-brown microcrystalline product (yield 95%). X-ray-quality crystals were obtained in CH_2Cl_2/pentane at 255 K. FT-IR (ν_{CO}, cm^{-1}): 2085.0, 2007.0 (CH_2Cl_2), 2075.0 (m br), 2062.5 (sh), 1987.3 (s), 1970.6 (sh), 1959.7 (sh) (ATR). ^{1}H NMR (298 K, 400.13 MHz, CD_2Cl_2, ppm): δ 3.28 (br s, N*H*), 2.99 (m, 4H, C*H*$_2$CH$_3$), 1.47 (t, 6H, CH$_2$C*H*$_3$, $^2J_{H-H}$ = 7.2 Hz). ^{13}C{^{1}H} NMR (298 K, 100.62 MHz, CD_2Cl_2, ppm): δ 183.5 (d, 1C, [Rh]−*C*O, $^1J_{C-Rh}$ = 65.7 Hz), 181.2 (d, 1C, [Rh]−*C*O, $^1J_{C-Rh}$ = 75.5 Hz), 49.4 (s, 1C, *C*H$_2$CH$_3$), 15.1 (s, 1C, CH$_2$*C*H$_3$). Anal. Calcd for $C_6H_{11}ClNO_2Rh$: C, 26.92; H, 4.11; N, 5.23. Found: C, 27.01; H, 4.19; N, 5.24. MS (DCI$^+$): m/z 285.0 [M + NH$_4$]$^+$ (100%).

*Chloro(dicarbonyl)(triethylamine)rhodium(I) Complex [RhCl(CO)$_2$(N(CH$_2$CH$_3$)$_3$)] (**3b**).* Dark oil (yield 78%). FT-IR (ν_{CO}, cm^{-1}): 2084.1, 2004.7 (CH_2Cl_2).

*Chloro(dicarbonyl)(imidazole)rhodium(I) Complex [RhCl(CO)$_2$(N$_2$C$_3$H$_4$)] (**3c**).* Red-orange microcrystalline product (yield 82%). FT-IR (ν_{CO}, cm^{-1}): 2085.6, 2009.6 (CH_2Cl_2). ^{1}H NMR (298 K, 300.18 MHz, CD_2Cl_2, ppm): δ 11.03 (br, 1H, =N*H*), 7.89 (br, 1H, ring N=C*H*−NH), 7.06 (s, 2H, ring N−C*H*=C*H*). ^{13}C{^{1}H} NMR (298 K, 75.48 MHz, CD_2Cl_2, ppm): δ 183.04 (br, 1C, [Rh]−CO), 137.85 (s, 1C, ring N=*C*H−NH), 129.18 (br, 1C, ring N−*C*H=CH), 117.42 (br, 1C, ring N−CH=*C*H).

*Chloro(dicarbonyl)(1-methylimidazole)rhodium(I) Complex [RhCl(CO)$_2$(N$_2$C$_4$H$_6$)] (**3d**).* Green-golden microcrystalline product (yield 93%). X-ray-quality crystals were obtained in CH_2Cl_2/pentane at 255 K. FT-IR (ν_{CO}, cm^{-1}): 2084.2, 2008.3 (CH_2Cl_2), 2074.2 (m), 2056.5 (s), 1995.5 (sh), 1983.8 (vs), 1970.7 (sh), 1958.7 (sh) (ATR). ^{1}H NMR (298 K, 400.13 MHz, CD_2Cl_2, ppm): δ 8.07 (s, 1H, ring N=C*H*N−CH$_3$), 7.21 (s, 1H, ring NC*H*=CHN−CH$_3$), 7.05 (s, 1H, ring NCH=C*H*N−CH$_3$), 3.77 (s, 3H, ring NCH=CHN-C*H*$_3$). ^{13}C{^{1}H} NMR (298 K, 100.62 MHz, CD_2Cl_2, ppm): δ 184.4 (d, 1C, [Rh]−*C*O, $^1J_{C-Rh}$ = 64.5 Hz), 181.2 (d, 1C, [Rh]−*C*O, $^1J_{C-Rh}$ = 73.9 Hz), 140.1 (s, 1C, ring N=*C*HN−CH$_3$), 130.4 (s, 1C, ring NCH=CHN−CH$_3$), 121.4 (s, 1C, ring NCH=CHN−CH$_3$), 34.8 (s, 1C, ring NCH=CHN−*C*H$_3$). Anal. Calcd for $C_6H_6ClN_2O_2Rh$: C, 26.05; H, 2.17; N, 10.13. Found: C, 26.10; H, 2.19; N, 10.15. MS (DCI$^+$): m/z 294.4 [M + NH$_4$]$^+$ (100%).

*Chloro(dicarbonyl)(pyrazole)rhodium(I) Complex [RhCl(CO)$_2$(N$_2$C$_3$H$_4$)] (**3e**).* Red microcrystalline product (yield 92%). X-ray-quality crystals were obtained in CH_2Cl_2/pentane at 255 K. FT-IR (ν_{CO}, cm^{-1}): 2089.9, 2017.3 (CH_2Cl_2), 2067.6 (s), 2009.0 (vs br), 1981.0 (sh) (ATR). ^{1}H NMR (298 K, CD_2Cl_2, 400.13 MHz, ppm): δ 9.18 (br s, 1H, ring N−N*H*−CH), 7.74 (s, 2H, ring C*H*$_a$=N−NH−C*H*$_b$), 6.56 (t, 1H, ring NH−CH=C*H*$_c$, $^3J_{H_c-H_a}$ = $^3J_{H_c-b}$ = 2.0 Hz). ^{13}C{^{1}H} NMR (298 K, 100.62 MHz, CD_2Cl_2, ppm): δ 182.1 (d, 2C, [Rh]−*C*O, $^1J_{C-Rh}$ = 70.8 Hz), 136.9 (br s, 2C, ring *C*H=N−NH−*C*H), 107.5 (s, 1C, ring NH−CH=*C*H). Anal. Calcd for $C_5H_4ClN_2O_2Rh$: C, 22.86; H, 1.52; N, 10.67. Found: C, 22.94; H, 1.60; N, 10.72. MS (DCI$^+$): m/z 280.4 [M + NH$_4$]$^+$ (100%).

*Chloro(dicarbonyl)(1-methylpyrazole)rhodium(I) Complex [RhCl(CO)$_2$(N$_2$C$_4$H$_6$)] (**3f**).* Red-orange microcrystalline product (yield 96%). X-ray-quality crystals were obtained in CH_2Cl_2/pentane at 255 K. FT-IR (ν_{CO}, cm^{-1}): 2089.7, 2015.5 (CH_2Cl_2), 2078.0 (vs), 1997.2 (vs) (ATR). ^{1}H NMR (298 K, CD_2Cl_2, 400.13 MHz, ppm): δ 7.69 (br d, 1H, ring N=C*H*$_b$−CH$_c$, $^3J_{H_b-H_c}$ = 2.0 Hz), 7.67 (br d, 1H, ring NCH$_3$−C*H*$_a$−CH$_c$, $^3J_{H_a-H_c}$ = 2.0 Hz), 6.45 (t, 1H, ring NCH$_3$−CH$_a$=C*H*$_c$, $^3J_{H-H}$ = 2.4 Hz), 4.16 (s, 3H, ring NC*H*$_3$). ^{13}C{^{1}H} NMR (298 K, 100.62 MHz, CD_2Cl_2, ppm): δ 183.3 (br d, 1C, [Rh]−*C*O, $^1J_{C-Rh}$ = 51.4 Hz,), 180.0 (br d, 1C, [Rh]−*C*O, $^1J_{C-Rh}$ = 60.1 Hz), 142.4 (s, 1C, ring N=*C*H), 134.3 (s, 1C, ring NCH$_3$−*C*H), 107.5 (s, 1C, ring NCH$_3$−*C*H=CH), 40.8 (s, 1C, ring N*C*H$_3$−CH). Anal. Calcd for $C_6H_6ClN_2O_2Rh$: C, 26.05; H, 2.17; N, 10.13. Found: C, 26.08; H, 2.18; N, 10.16. MS (DCI$^+$): m/z 294.3 [M + NH$_4$]$^+$ (100%).

*Chloro(dicarbonyl)(3,5-dimethylpyrazole)rhodium(I) Complex [RhCl(CO)$_2$(N$_2$C$_5$H$_8$)] (**3g**).* Red microcrystalline product (yield 91%). FT-IR (ν_{CO}, cm^{-1}): 2087.9, 2013.9 (CH_2Cl_2). ^{1}H NMR (298 K, 300.18 MHz, CD_2Cl_2, ppm): δ 11.23 (br s 1H, ring N−N*H*−C(CH$_3$)), 5.98 (s, 1H, ring N=C(CH$_3$)−C*H*), 2.37 (br s, 3H, −CH$_3$, ring (CH$_3$)−C=N−NH−C(CH$_3$)), 2.24 (br s, 3H, −CH$_3$, ring (CH$_3$)−C=N−NH−C(CH$_3$)). ^{13}C{^{1}H} NMR (298 K, 75.48 MHz, CD_2Cl_2, ppm): δ 183.81 (d, 1C, [Rh]−*C*O, $^1J_{C-Rh}$ = 62.0 Hz), 180.6 (d, 1C, [Rh]−*C*O, $^1J_{C-Rh}$ = 80.2 Hz), 152.53 (s, 1C, =*C*<, ring (CH$_3$)−*C*=N−NH−C(CH$_3$)), 142.65 (s, 1C, =*C*<, ring (CH$_3$)−*C*=N−NH−C(CH$_3$)), 105.91 (s, 1C, ring N=*C*(CH$_3$)−CH), 15.09 (s, 1C, −CH$_3$, ring (CH$_3$)−C=N−NH−C(*C*H$_3$)), 10.86 (s, 1C, −CH$_3$, ring (*C*H$_3$)−C=N−NH−C(CH$_3$)).

*Chloro(dicarbonyl)(diethylsulfide)rhodium(I) Complex [RhCl(CO)$_2$(S(CH$_2$CH$_3$)$_2$)] (**3h**).* Red oil (yield 84%). FT-IR (ν_{CO}, cm^{-1}): 2091.0, 2014.9 (CH_2Cl_2). ^{1}H NMR (298 K, 300.18 MHz, CD_2Cl_2, ppm): δ 2.90 (q, 4H, S(*C*H$_2$−CH$_3$)$_2$, $^3J_{H-H}$ = 7.5 Hz), 1.30 (t, 6H, S(CH$_2$−*C*H$_3$)$_2$, $^3J_{H-H}$ = 7.5 Hz). ^{13}C{^{1}H} NMR (298 K, 75.48 MHz, CD_2Cl_2, ppm): δ 180.55 (d, 2C, [Rh]−*C*O, $^1J_{C-Rh}$ = 67.9 Hz), 29.40 (s, 2C, S(*C*H$_2$−CH$_3$)$_2$), 13.60 (s, 2C, S(CH$_2$−*C*H$_3$)$_2$).

Synthesis of Neutral *cis*-4 Complexes. To a dichloromethane solution (V = 25 mL) of **2** (500 mg, 0.87 mmol) under stirring was added via canulation a solution of 2 mol equiv of ligand (**a**−**h**) in dichloromethane (V = 5 mL) at 263 K. The reaction mixture was slowly warmed to room temperature and vigorously stirred for 6 h. After solvent removal under vacuum, compounds **4** were washed with pentane, dried under vacuum, and stored under argon at 255 K prior to use. For ^{13}C{^{1}H} NMR measurements of **4** and **6**, ^{13}CO-labeled **2** was used as the precursor.

*Iodo(dicarbonyl)(diethylamine)rhodium(I) Complex [RhI(CO)$_2$(HN(CH$_2$CH$_3$)$_2$)] (**4a**).* Brown-green microcrystalline product (yield 92%). X-ray-quality crystals were obtained in pentane at 255 K. FT-IR (ν_{CO}, cm^{-1}): 2077.6, 2005.8 (CH_2Cl_2), 2074.0, 2000.9 (CH_3I), 2068.1 (m br), 1998.3 (vs) (ATR). **4a-^{13}CO**. ^{1}H NMR (298 K, 400.13 MHz, CD_2Cl_2, ppm): δ 3.45 (br s, 1H, N*H*), 3.07 (m, 2H, C*H*$_2$CH$_3$, $^2J_{H-H}$ = 4.0 Hz), 2.97 (m, 2H, C*H*$_2$CH$_3$, $^2J_{H-H}$ = 4.0 Hz), 1.45 (t, 6H, CH$_2$C*H*$_3$, $^2J_{H-H}$ = 6.4 Hz). ^{13}C{^{1}H} NMR (298 K, 100.62 MHz, CD_2Cl_2, ppm): δ 184.5 (dd, 1C, [Rh]−*C*O, $^1J_{C-Rh}$ = 65.4 Hz, $^2J_{C-C}$ = 4.0 Hz), 180.2 (dd, 1C, [Rh]−*C*O, $^1J_{C-Rh}$ = 79.5 Hz, $^2J_{C-C}$ = 4.1 Hz), 49.8 (s, 1C, *C*H$_2$CH$_3$), 15.1 (s, 1C, CH$_2$*C*H$_3$). Anal. Calcd for $C_6H_{11}INO_2Rh$: C, 20.05; H, 3.06; N, 3.90. Found: C, 20.20; H, 3.22; N, 3.70. MS (DCI$^+$): m/z 376.9 [M + NH$_4$]$^+$ (100%).

*Iodo(dicarbonyl)(triethylamine)rhodium(I) Complex [RhI(CO)$_2$(N(CH$_2$CH$_3$)$_3$)] (**4b**).* Dark-brown oil (yield 80%). FT-IR (ν_{CO}, cm^{-1}): 2076.4, 2003.5 (CH_2Cl_2), 2057.4, 1984.7 (ATR).

dx.doi.org/10.1021/ic2019988 | Inorg. Chem. 2012, 51, 8670−8685

*Iodo(dicarbonyl)(imidazole)rhodium(I) Complex [RhI(CO)$_2$(N$_2$C$_3$H$_4$)] (**4c**).* Brown microcrystalline product (yield 89%). FT-IR (ν_{CO}, cm^{-1}): 2077.9, 2008.1 (CH_2Cl_2), 2073.3, 2002.8 (CH_3I), 2076.0 (sh), 2059.5 (vs), 1996.1 (vs br), 1970.6 (sh) (ATR). **4c-^{13}CO**. ^{1}H NMR (298 K, 500.33 MHz, CD_3OD, ppm): δ 8.26 (s, 1H, ring N=C*H*−NH), 7.33 (br s, 1H, ring N−C*H*=CH), 7.24 (br s, 1H, ring N−CH=C*H*). ^{13}C{^{1}H} NMR (298 K, 125.82 MHz, CD_3OD, ppm): δ 185.7 (br d, 1C, [Rh]−*C*O, $^1J_{C-Rh}$ = 63.2 Hz), 180.0 (br d, 1C, [Rh]−*C*O, $^1J_{C-Rh}$ = 70.8 Hz), 140.3 (s, 1C, ring N=*C*H−NH), 130.5 (s, 1C, ring N−*C*H=CH), 117.1 (s, 1C, ring N−CH=*C*H). ^{1}H NMR (233 K, 500.33 MHz, CD_3OD, ppm): δ 8.36 (s, 1H, ring N=CH_a−NH), 7.40 (s, 1H, ring N−CH_b=CH_c), 7.28 (t, 1H, ring N−CH_b=CH_c, $^3J_{H_c-H_b}$ = $^4J_{H_c-H_a}$ = 1.5 Hz). ^{13}C{^{1}H} NMR (233 K, 125.82 MHz, CD_3OD, ppm): δ 186.1 (d, 1C, [Rh]−*C*O, $^1J_{C-Rh}$ = 61.9 Hz), 179.9 (d, 1C, [Rh]−*C*O, $^1J_{C-Rh}$ = 76.5 Hz), 140.6 (s, 1C, ring N=*C*H−NH), 130.8 (s, 1C, ring N−*C*H=CH), 117.2 (s, 1C, ring N−CH=*C*H). Anal. Calcd for $C_5H_4IN_2O_2Rh$: C, 18.75; H, 1.25; N, 8.75. Found: C, 18.74; H, 1.22; N, 8.74. MS (DCI$^+$): m/z 371.8 [M + NH$_4$]$^+$ (100%).

*Iodo(dicarbonyl)(1-methylimidazole)rhodium(I) Complex [RhI(CO)$_2$(N$_2$C$_4$H$_6$)] (**4d**).* Brown microcrystalline product (yield 92%). X-ray-quality crystals were obtained in CH_2Cl_2/pentane at 255 K. FT-IR (ν_{CO}, cm^{-1}): 2077.0, 2007.1 (CH_2Cl_2), 2072.4, 2002.0 (CH_3I), 2052.2 (s), 1994.6 (vs br) (ATR). **4d-^{13}CO**. ^{1}H NMR (298 K, CD_2Cl_2, 500.33 MHz, ppm): δ 8.14 (s, 1H, ring N=C*H*N−CH_3), 7.30 (s, 1H, ring NC*H*=CHN−CH_3), 7.03 (s, 1H, ring NCH=C*H*N−CH_3), 3.78 (s, 3H, ring NCH=CHN−CH_3). ^{13}C{^{1}H} NMR (298 K, 125.82 MHz, CD_2Cl_2, ppm): δ 185.0 (br d, 1C, [Rh]−*C*O), 180.1 (br d, 1C, [Rh]−*C*O, $^1J_{C-Rh}$ = 73.0 Hz), 142.3 (s, 1C, ring N=*C*HN−CH_3), 131.9 (s, 1C, ring NCH=*C*HN−CH_3), 121.4 (s, 1C, ring NCH=*C*HN−CH_3), 34.7 (s, 1C, ring NCH=CHN−*C*H$_3$). ^{1}H NMR (235 K, CD_2Cl_2, 500.33 MHz, ppm): δ 8.12 (s, 1H, ring N=C*H*N−CH_3), 7.25 (s, 1H, ring NC*H*=CHN−CH_3), 7.04 (d, 1H, ring NCH=C*H*N−CH_3, $^3J_{H-H}$ = 1.5 Hz), 3.76 (br s, 3H, ring NCH=CHN−CH_3, $^2J_{H-N}$ = 3.5 Hz). ^{13}C{^{1}H} NMR (235 K, 125.82 MHz, CD_2Cl_2, ppm): δ 185.4 (d, 1C, [Rh]−*C*O, $^1J_{C-Rh}$ = 62.4 Hz), 179.8 (d, 1C, [Rh]−*C*O, $^1J_{C-Rh}$ = 77.9 Hz), 142.3 (s, 1C, ring N=*C*HN−CH_3), 131.9 (s, 1C, ring NCH=*C*HN−CH_3), 121.6 (s, 1C, ring NCH=*C*HN−CH_3), 35.0 (s, 1C, ring NCH=CHN−*C*H$_3$). ^{1}H NMR (298 K, CD_3OD, 500.33 MHz, ppm): δ 8.22 (s, 1H, ring N=C*H*N−CH_3), 7.31 (s, 1H, ring NC*H*=CHN−CH_3), 7.22 (s, 1H, ring NCH=C*H*N−CH_3), 3.80 (s, 3H, ring NCH=CHN-CH_3). ^{13}C{^{1}H} NMR (298 K, 125.82 MHz, CD_3OD, ppm): δ 185.5 (br d, 1C, [Rh]−*C*O), 180.1 (br d, 1C, [Rh]−*C*O), 142.3 (s, 1C, ring N=*C*HN−CH_3), 131.2 (s, 1C, ring NCH=*C*HN−CH_3), 121.6 (s, 1C, ring NCH=*C*HN−CH_3), 33.4 (s, 1C, ring NCH=CHN-*C*H$_3$). ^{1}H NMR (243 K, CD_3OD, 500.33 MHz, ppm): δ 8.30 (s, 1H, ring N=C*H*N−CH_3), 7.38 (s, 1H, ring NC*H*=CHN−CH_3), 7.26 (d, 1H, ring NCH=C*H*N−CH_3), 3.81 (br s, 3H, ring NCH=CHN−CH_3). ^{13}C{^{1}H} NMR (243 K, 125.82 MHz, CD_3OD, ppm): δ 185.9 (d, 1C, [Rh]−*C*O, $^1J_{C-Rh}$ = 62.0 Hz), 179.9 (d, 1C, [Rh]−*C*O, $^1J_{C-Rh}$ = 76.5 Hz), 142.6 (s, 1C, ring N=*C*HN−CH_3), 131.5 (s, 1C, ring NCH=*C*HN−CH_3), 121.5 (s, 1C, ring NCH=*C*HN−CH_3), 33.4 (s, 1C, ring NCH=CHN−*C*H$_3$). 2D (^{1}H−^{15}N) HMBC NMR (298 K, CD_2Cl_2, 500.33−50.70 MHz, ppm): δ −214.2 (br s, 1N, ring N=CH*N*−CH_3, $^2J_{N-H}$ = 6.6 Hz), −189.8 (br d, 1N, ring *N*=CHN−CH_3, $^1J_{Rh-N}$ = 23.5 Hz). Anal. Calcd for $C_6H_6IN_2O_2Rh$: C, 19.57; H, 1.64; N, 7.55. Found: C, 19.17; H, 1.63; N, 7.61. MS (DCI$^+$): m/z 385.9 [M + NH$_4$]$^+$ (100%).

*Iodo(dicarbonyl)(pyrazole)rhodium(I) Complex [RhI(CO)$_2$(N$_2$C$_3$H$_4$)] (**4e**).* Brown-orange microcrystalline product (yield 95%). X-ray-quality crystals were obtained in CH_2Cl_2/pentane at 255 K. FT-IR (ν_{CO}, cm^{-1}): 2082.4, 2015.0 (CH_2Cl_2), 2078.0, 2010.3 (CH_3I), 2060.2 (s), 1999.4 (vs br), 1976.8 (sh), 1967.7 (sh), 1904.4 (sh) (ATR). **4e-^{13}CO**. ^{1}H NMR (298 K, CD_2Cl_2, 500.33 MHz, ppm): δ 11.71 (br s, 1H, ring N−N*H*−CH), 7.78 (br s, 2H, ring CH_a=N−NH−CH_b), 6.54 (t, 1H, ring NH−CH=CH_c, $^3J_{H_c-H_a}$ = $^3J_{H_c-H_b}$ = 2.5 Hz). ^{13}C{^{1}H} NMR (298 K, 125.82 MHz, CD_2Cl_2, ppm): δ 181.7 (br s, 2C, [Rh]−*C*O), 144.9 (br s, 1C, ring *C*H=N−NH), 131.4 (br s, 1C, ring N−NH−*C*H), 107.8 (s, 1C, ring NH−*C*H=CH). ^{1}H NMR (223 K, CD_2Cl_2, 500.33 MHz, ppm): δ 11.68 (br s, 1H, ring N−N*H*−CH), 7.77 (s, 1H, ring CH_a=N−NH), 7.72 (s, 1H, ring N−NH−CH_b), 6.51 (s, 1H, ring NH−CH=CH_c). ^{13}C{^{1}H} NMR (223 K, 125.82 MHz, CD_2Cl_2, ppm): δ 184.9 (dd, 1C, [Rh]−*C*O, $^1J_{C-Rh}$ = 62.9 Hz, $^2J_{C-C}$ = 4.4 Hz), 179.1 (dd, 1C, [Rh]−*C*O, $^1J_{C-Rh}$ = 78.0 Hz, $^2J_{C-C}$ = 5.2 Hz), 145.2 (s, 1C, ring *C*H=N−NH), 131.8 (s, 1C, ring N−NH−*C*H), 108.1 (s, 1C, ring NH−*C*H=CH). 2D (^{1}H−^{15}N) HMBC NMR (250 K, CD_2Cl_2, 500.33−50.70 MHz, ppm): δ −171.3 (br s, 1N, ring N−*N*H−CH), −158.7 (br d, 1N, ring *N*−NH−CH). 2D (^{1}H−^{103}Rh) HMQC NMR (243 K, CD_2Cl_2, 500.33−15.82 MHz, ppm): δ −8387 (br s, Rh). Anal. Calcd for $C_5H_4IN_2O_2Rh$: C, 16.87; H, 1.06; N, 8.01. Found: C, 16.95; H, 1.13; N, 7.91. MS (DCI$^+$): m/z 371.9 [M + NH$_4$]$^+$ (100%).

*Iodo(dicarbonyl)(1-methylpyrazole)rhodium(I) Complex [RhI(CO)$_2$(N$_2$C$_4$H$_6$)] (**4f**).* Bright-yellow microcrystalline product (yield 94%). X-ray-quality crystals were obtained in CH_2Cl_2/pentane at 255 K. FT-IR (ν_{CO}, cm^{-1}): 2082.0, 2013.4 (CH_2Cl_2), 2077.6, 2009.2 (CH_3I), 2056.3 (vs), 1986.4 (vs), 1971.0 (sh), 1963.5 (sh) (ATR). **4f-^{13}CO**. ^{1}H NMR (298 K, CD_2Cl_2, 500.33 MHz, ppm): δ 7.69 (br d, 1H, ring N=CH_b−CH_c, $^3J_{H_b-H_c}$ = 2.0 Hz), 7.65 (br d, 1H, ring NCH$_3$−CH_a−CH_c, $^3J_{H_a-H_c}$ = 2.0 Hz), 6.50 (t, 1H, ring NCH$_3$−CH$_a$=CH_c, $^3J_{H-H}$ = 2.5 Hz), 4.16 (s, 3H, ring NCH_3). ^{13}C{^{1}H} NMR (298 K, 125.82 MHz, CD_2Cl_2, ppm): δ 182.0 (br s, 1C, [Rh]−*C*O), 142.8 (s, 1C, ring N=*C*H), 134.2 (s, 1C, ring NCH$_3$−*C*H), 107.8 (s, 1C, ring NCH$_3$−CH=*C*H), 41.3 (s, 1C, ring N*C*H$_3$−CH). ^{1}H NMR (203 K, CD_2Cl_2, 500.33 MHz, ppm): δ 7.66 (br d, 1H, ring NCH$_3$−CH_a=CH$_c$, $^3J_{H_a-H_c}$ = 2.0 Hz), 7.65 (br d, 1H, ring N=CH_b−CH$_c$, $^3J_{H_b-H_c}$ = 2.0 Hz), 6.47 (t, 1H, ring NCH$_3$−CH$_a$=CH_c, $^3J_{H-H}$ = 2.5 Hz), 4.10 (s, 3H, ring NCH_3). ^{13}C{^{1}H} NMR (203 K, 125.82 MHz, CD_2Cl_2, ppm): δ 185.2 (dd, 1C, [Rh]−*C*O, $^1J_{C-Rh}$ = 59.1 Hz, $^2J_{C-C}$ = 4.8 Hz), 178.9 (dd, 1C, [Rh]−*C*O, $^1J_{C-Rh}$ = 75.5 Hz, $^2J_{C-C}$ = 4.8 Hz), 142.7 (s, 1C, ring N=*C*H), 134.5 (s, 1C, ring NCH$_3$−*C*H), 107.9 (s, 1C, ring NCH$_3$−CH=*C*H), 41.7 (s, 1C, ring N*C*H$_3$−CH). 2D (^{1}H−^{15}N) HMBC NMR (298 K, CD_2Cl_2, 500.33−50.70 MHz, ppm): δ −178.6 (br s, 1N, ring N−*N*CH$_3$), −153.9 (br d, 1N, ring *N*−NCH$_3$). 2D (^{1}H−^{103}Rh) HMQC NMR (243 K, CD_2Cl_2, 500.33−15.82 MHz, ppm): δ −8334 (br s, Rh). Anal. Calcd for $C_6H_6IN_2O_2Rh$: C, 19.36; H, 1.65; N, 7.43. Found: C, 19.57; H, 1.63; N, 7.61. MS (DCI$^+$): m/z 385.9 [M + NH$_4$]$^+$ (100%).

*Iodo(dicarbonyl)(3,5-dimethylpyrazole)rhodium(I) Complex [RhI(CO)$_2$(N$_2$C$_5$H$_8$)] (**4g**).* Dark-green microcrystalline product (yield 96%). FT-IR (ν_{CO}, cm^{-1}): 2080.2, 2011.9 (CH_2Cl_2), 2075.6, 2007.1 (CH_3I), 2070.0 (vs), 2005.8 (vs br) (ATR). **4g-^{13}CO**. ^{1}H NMR (298 K, 500.33 MHz, CD_2Cl_2, ppm): δ 9.83 (br s 1H, ring N−N*H*−C(CH$_3$)), 5.43 (s, 1H, ring N=C(CH$_3$)−C*H*), 1.72 (br s, 6H, ring (C*H*$_3$)−C=N−NH−C(C*H*$_3$)). ^{13}C{^{1}H} NMR (298 K, 125.82 MHz, CD_2Cl_2, ppm): δ 181.4 (br s, 2C, [Rh]−*C*O), 142.6 (br s, 2C, ring (CH$_3$)−*C*=N−NH−*C*(CH$_3$)), 106.0 (s, 1C, ring N=*C*(CH$_3$)−CH), 13.6 (s, 1C, ring (*C*H$_3$)−C=N−NH−C(*C*H$_3$)), 10.3 (s, 1C, ring (*C*H$_3$)−C=N−NH−C(*C*H$_3$)). ^{1}H NMR (193 K, 500.33 MHz, CD_2Cl_2, ppm): δ 9.97 (s 1H, ring N−N*H*−C(CH$_3$)), 5.41 (s, 1H, ring N=C(CH$_3$)−C*H*), 1.76 (s, 3H, ring (C*H*$_3$)−C=N−NH−C(CH$_3$)), 1.65 (s, 3H, ring (CH$_3$)−C=N−NH−C(C*H*$_3$)). ^{13}C{^{1}H} NMR (193 K, 125.82 MHz, CD_2Cl_2, ppm): δ 184.6 (d, 1C, [Rh]−*C*O, $^1J_{C-Rh}$ = 62.9 Hz), 178.2 (d, 1C, [Rh]−*C*O, $^1J_{C-Rh}$ = 78.0 Hz), 151.7 (s, 1C, ring (CH$_3$)−*C*=N−NH−C(CH$_3$)), 142.8 (s, 1C, ring (CH$_3$)−*C*=N−NH−*C*(CH$_3$)), 105.9 (s, 1C, ring N=*C*(CH$_3$)−CH), 15.3 (s, 1C, ring (*C*H$_3$)−C=N−NH−C(*C*H$_3$)), 10.7 (s, 1C, ring (*C*H$_3$)−C=N−NH−C(*C*H$_3$)). Anal. Calcd for $C_7H_8IN_2O_2Rh$: C, 21.89; H, 1.97; N, 7.27. Found: C, 21.99; H, 2.09; N, 7.33. MS (DCI$^+$): m/z 399.9 [M + NH$_4$]$^+$ (100%).

*Iodo(dicarbonyl)(diethylsulfide)rhodium(I) Complex [RhI(CO)$_2$(S(CH$_2$CH$_3$)$_2$)] (**4h**).* Red powder (yield 87%). FT-IR (ν_{CO}, cm^{-1}): 2081.3, 2013.4 (CH_2Cl_2), 2077.3, 2008.3 (CH_3I), 2067.0 (vs), 1997.7 (vs), 1968.5 (sh) (ATR). **4h-^{13}CO**. ^{1}H NMR (298 K, 500.33 MHz, CD_2Cl_2, ppm): δ 3.08 (q, 4H, S(CH_2−CH$_3$)$_2$, $^3J_{H-H}$ = 7.5 Hz), 1.45 (t, 6H, S(CH$_2$−CH_3)$_2$, $^3J_{H-H}$ = 7.5 Hz). ^{13}C{^{1}H} NMR (298 K, 125.82 MHz, CD_2Cl_2, ppm): δ 180.8 (br d, 2C, [Rh]−*C*O, $^1J_{C-Rh}$ = 67.4 Hz), 31.6 (s, 2C, S(*C*H$_2$−CH$_3$)$_2$), 13.8 (s, 2C, S(CH$_2$−*C*H$_3$)$_2$). ^{1}H NMR (183 K, 500.33 MHz, CD_2Cl_2, ppm): δ 3.06 (br d, 4H, S(CH_2−CH$_3$)$_2$, $^3J_{H-H}$ = 6.0 Hz), 1.36 (t, 6H, S(CH$_2$−CH_3)$_2$, $^3J_{H-H}$ = 7.5 Hz).

dx.doi.org/10.1021/ic2019988 | *Inorg. Chem.* 2012, 51, 8670−8685

$^{13}C\{^1H\}$ NMR (183 K, 125.82 MHz, CD_2Cl_2, ppm): δ 182.5 (d, 1C, [Rh]−*C*O, $^1J_{C-Rh}$ = 66.7 Hz), 180.1 (d, 1C, [Rh]−*C*O, $^1J_{C-Rh}$ = 76.8 Hz), 30.2 (s, 2C, S(CH_2−CH_3)$_2$), 14.2 (s, 2C, S(CH_2−CH_3)$_2$). Anal. Calcd for $C_6H_{10}SIO_2Rh$: C, 19.15; H, 2.66; S, 8.51. Found: C, 19.30; H, 2.70; S, 8.62. MS (DCI$^+$): *m*/*z* 393.99 [M + NH_4]$^+$ (100%).

Synthesis of Neutral Rhodium(III) Complex [RhI(μ-I)(COMe)(CO)(NCMe)]$_2$ (5).[29] **2** (0.46 g, 0.80 mmol) was dissolved in MeCN/MeI (50 mL, 2:1, v/v) and stirred at room temperature under argon for 6 h. The volatile portion was removed under vacuum, and the resulting orange-red precipitate was dried and stored under argon at 255 K prior to use. Orange-red microcrystalline product (yield 90%). FT-IR (ν_{CO}, ν_{COMe}, cm^{-1}): 2090.8, 1749.2, 1730.7 (CH_2Cl_2), 2080.1, 1702.3 (ATR). ^1H NMR (298 K, 400.13 MHz, CD_2Cl_2, ppm): δ 2.92 (br s, 6H, COCH_3), 2.65 (br s, 6H, NC−CH_3). $^{13}C\{^1H\}$ NMR (298 K, 100.62 MHz, CD_2Cl_2, ppm): δ 207.9 (d, 2C, [Rh]−*C*OCH$_3$, $^1J_{C-Rh}$ = 18.9 Hz), 182.1 (d, 2C, [Rh]−*C*O, $^1J_{C-Rh}$ = 63.7 Hz), 58.7 (s, 2C, NC−CH_3), 45.6 (s, 2C, COCH_3), 29.7 (s, 2C, NC−CH_3). Anal. Calcd for $C_5H_6I_2NO_2Rh$: C, 12.80; H, 1.28; N, 2.98. Found: C, 12.91; H, 1.32; N, 2.92.

Synthesis of Neutral Rhodium(III) Complexes [RhI(μ-I)(COMe)(CO)(L)]$_2$ (6). To a solution of MeI (12 mL) was added *cis*-**4** (200 mg) at room temperature. The solution was allowed to react at room temperature under vigorous stirring for 5 days (in order to make sure that the oxidative addition was complete). During this time, all solutions turned dark red. After removal of MeI excess under vacuum, the compounds **6a** and **6c**−**6h** obtained were washed with pentane or ether, dried under vacuum, and stored under argon at 255 K prior to use.

[RhI(μ-I)(COMe)(CO)(HN(CH_2CH_3)$_2$)]$_2$ ***(6a)***. Dark-brown oil (yield 87%). FT-IR (ν_{CO}, ν_{COMe}, cm^{-1}): 2072.6, 1719.1 (CH_2Cl_2), 2063.3, 1716.4 (CH_3I). ^1H NMR (298 K, 400.13 MHz, CD_2Cl_2, ppm): δ 7.68 (br s, 2H, N*H*), 3.18 (q, 8H, CH_2CH$_3$, $^2J_{H-H}$ = 6.2 Hz), 3.15 (s, 6H, COCH_3), 1.44 (t, 12H, CH_2CH_3, $^2J_{H-H}$ = 7.2 Hz). $^{13}C\{^1H\}$ NMR (298 K, 100.62 MHz, CD_2Cl_2, ppm): δ not observed (*C*OMe), 188−182 (br m, main d at 183.4, *C*O, $^1J_{C-Rh}$ = 72.9 Hz), 49.7 (br s, 2C, COCH_3), 42.9 (s, 4C, CH_2CH_3), 11.1 (s, 4C, CH_2CH_3).

[RhI(μ-I)(COMe)(CO)($N_2C_3H_4$)]$_2$ ***(6c)***. Dark-brown powder poorly soluble in CH_2Cl_2 (yield 86%). FT-IR (ν_{CO}, ν_{COMe}, cm^{-1}): 2073.7, 1734.9, 1707.0 (CH_2Cl_2), 2073.9, 1719.2, 1705.2 (CH_3I). ^1H NMR (298 K, 300.13 MHz, CD_2Cl_2, ppm): δ 9.66 (br s, 2H, ring N=CH−N*H*), 8.77 (s, 2H, ring N=C*H*−NH), 8.02 (s, 2H, ring N−C*H*=CH), 7.14 (s, 2H, ring N−CH=C*H*). Anal. Calcd for $C_6H_7I_2N_2O_2Rh$: C, 14.52; H, 1.41; N, 5.64. Found: C, 14.68; H, 1.60; N, 5.52.

[RhI(μ-I)(COMe)(CO)($N_2C_4H_6$)]$_2$ ***(6d)***. Red microcrystalline product (yield 88%). X-ray-quality crystals were obtained in CH_2Cl_2 at 255 K. FT-IR (ν_{CO}, ν_{COMe}, cm^{-1}): 2073.1, 1733.5 (CH_2Cl_2), 2068.0, 1736.0 (CH_3I). **6d-^{13}CO**. ^1H NMR (298 K, CD_2Cl_2, 400.13 MHz, ppm): δ 8.58 (s, 2H, ring N=C*H*N−CH_3), 7.96 (s, 2H, ring NC*H*=CHN−CH_3), 6.98 (s, 2H, ring NCH=C*H*N−CH_3), 3.85 (br s, 6H, ring NCH=CHN−CH_3), 2.84 (br s, 6H, COCH_3). $^{13}C\{^1H\}$ NMR (298 K, 100.62 MHz, CD_2Cl_2, ppm): δ 216−208 (br m, [Rh]−*C*OMe, main pseudo-d at 209.8, $^1J_{C-Rh}$ = 17.6 Hz), 185−179 (br m, [Rh]−*C*O, main d at 183.4, $^1J_{C-Rh}$ = 58.3 Hz), 145.0 (s, 1C, ring N=*C*HN−CH_3), 134.5 (s, 1C, ring NCH=*C*HN−CH_3), 120.5 (s, 1C, ring NCH=*C*HN−CH_3), 47.3 (m, 2C, COCH_3), 34.7 (s, 2C, ring NCH=CHN−CH_3). Anal. Calcd for $C_7H_9I_2N_2O_2Rh$: C, 16.48; H, 1.76; N, 5.49. Found: C, 16.82; H, 1.90; N, 5.39.

[RhI(μ-I)(COMe)(CO)($N_2C_3H_4$)]$_2$ ***(6e)***. Red microcrystalline product (yield 90%). X-ray-quality crystals were obtained in CH_2Cl_2 at 255 K. FT-IR (ν_{CO}, ν_{COMe}, cm^{-1}): 2083.5, 1741.0, 1721.0 (CH_2Cl_2); 2075.6, 1736.7 (CH_3I). **6e-^{13}CO**. ^1H NMR (298 K, CD_2Cl_2, 300.13 MHz, ppm): δ 11.84 (br s, 2H, ring N−N*H*−CH), 7.81 (br s, 2H, ring C*H*=N−NH−CH), 7.75 (s, 2H, ring CH=N−NH−C*H*), 6.55 (t, 2H, ring NH−CH=C*H*, $^3J_{H-H}$ = 2.4 Hz), 2.95, 2.94 (6H, COCH_3). $^{13}C\{^1H\}$ NMR (298 K, 75.47 MHz, CD_2Cl_2, ppm): δ 213.2 (br s, [Rh]−*C*OMe), 186−178 (br m, main d at 182.8, [Rh]−*C*O, $^1J_{C-Rh}$ = 60.6 Hz), 146.1 (s, 2C, ring *C*H=N−NH), 131.3 (s, 2C, ring N−NH−*C*H), 107.6 (s, 2C, ring NH−*C*H=*C*H), 48.0 (br s 2C, COCH$_3$). Anal. Calcd for $C_6H_7I_2N_2O_2Rh$: C, 14.52; H, 1.41; N, 5.64. Found: C, 14.41; H, 1.43; N, 5.59.

[RhI(μ-I)(COMe)(CO)($N_2C_4H_6$)]$_2$ ***(6f)***. Dark-brown powder (yield 84%). FT-IR (ν_{CO}, ν_{COMe}, cm^{-1}): 2076.6, 1778.0 (CH_2Cl_2), 2072.3, 1776.4, 1743.7 (CH_3I). ^1H NMR (298 K, CD_2Cl_2, 300.13 MHz, ppm): δ 8.21 (br s, 1H, ring N=C*H*−CH), 7.89 (br s, 1H, ring N=C*H*−CH), 7.73 (br s, 1H, ring NCH_3−C*H*−CH), 7.60 (br s, 1H, ring NCH_3−C*H*−CH), 6.59 (br s, 1H, ring NCH_3−CH=C*H*), 6.44 (br s, 1H, ring NCH_3−CH=C*H*), 3.97 (s, 6H, ring NCH_3), 3.75 (s, 3H, COCH_3), 3.17 (s, 3H, COCH_3). $^{13}C\{^1H\}$ NMR (298 K, 75.47 MHz, CD_2Cl_2, ppm): δ not observed ([Rh]−*C*OMe), 182.0 (br d, [Rh]−*C*O, $^1J_{C-Rh}$ = 65.7 Hz), 148.7 (s, 1C, ring N=*C*H), 145.3 (s, 1C, ring N=*C*H), 138.1 (s, 1C, ring NCH_3−*C*H), 135.2 (s, 1C, ring NCH_3−*C*H), 107.7 (s, 1C, ring NCH_3−CH=*C*H), 106.6 (s, 1C, ring NCH_3−CH=*C*H), 45.5 (br s, 2C, COCH_3), 37.8 (s, 2C, ring NCH_3−CH). Anal. Calcd for $C_7H_9I_2N_2O_2Rh$: C, 16.48; H, 1.76; N, 5.49. Found: C, 16.64; H, 1.83; N, 5.41.

[RhI(μ-I)(COMe)(CO)($N_2C_5H_8$)]$_2$ ***(6g)***. Dark-brown powder (yield 86%). FT-IR (ν_{CO}, ν_{COMe}, cm^{-1}): 2079.6, 1753.8 (CH_2Cl_2), 2075.5, 1749.6 (CH_3I). ^1H NMR (298 K, 300.13 MHz, CD_2Cl_2, ppm): δ 10.82 (br s 2H, ring N−N*H*−C(CH_3)), 6.08 (br s, 2H, ring N=C(CH_3)−C*H*), 3.18 (s, 6H, COCH_3), 2.44 (s, 6H, ring1 (CH_3)−C=N−NH−C(CH_3)), 2.25 (s, 6H, ring2 (CH_3)−C=N−NH−C(CH_3)). $^{13}C\{^1H\}$ NMR (298 K, 100.62 MHz, CD_2Cl_2, ppm): δ 212.5 (d, [Rh]−*C*OMe, $^1J_{C-Rh}$ = 19.0 Hz), 204.6 (br m, [Rh]−*C*OMe), 183.6 (d, [Rh]−*C*O, $^1J_{C-Rh}$ = 63.1 Hz), 150.9 (s, 2C, ring (CH_3)−C=N−NH−C(CH_3)), 142.5 (s, 2C, ring (CH_3)−C=N−NH−*C*(CH_3)), 107.6 (s, 2C, ring N=C(CH_3)−*C*H), 46.5 (br s, 2C, COCH_3), 16.2 (s, 2C, ring (*C*H$_3$)−C=N−NH−C(CH_3)), 11.1 (s, 2C, ring (CH_3)−C=N−NH−C(*C*H$_3$)). Anal. Calcd for $C_8H_{11}I_2N_2O_2Rh$: C, 18.33; H, 2.10; N, 5.34. Found: C, 18.60; H, 2.37; N, 5.21.

[RhI(μ-I)(COMe)(CO)(S(CH_2CH_3)$_2$)]$_2$ ***(6h)***. Red powder (yield 85%). FT-IR (ν_{CO}, ν_{COMe}, cm^{-1}): 2080.6, 1720.8 (CH_2Cl_2), 2076.4, 1743.6 (CH_3I). ^1H NMR (298 K, 300.18 MHz, CD_2Cl_2, ppm): δ 3.33 (br q, 8H, >CH_2, S(CH_2CH$_3$)$_2$, J_{H-H} = 6.9 Hz), 3.02 (br s, −CH_3, [Rh]−COCH_3), 1.44 (t, 12H, −CH_3, S(CH_2CH_3)$_2$, J_{H-H} = 7.5 Hz). $^{13}C\{^1H\}$ NMR (298 K, 75.480 MHz, CD_2Cl_2, ppm): δ not observed ([Rh]−*C*OCH$_3$ and [Rh]−*C*O), 47.71 (s, [Rh]−CO*C*H$_3$), 33.91 (s, >CH_2, S(CH_2CH_3)$_2$), 14.62 (s, −CH_3, S(CH_2CH_3)$_2$). Anal. Calcd for $C_7H_{13}I_2SO_2Rh$: C, 16.22; H, 2.51; S, 6.19. Found: C, 16.41; H, 2.71; S, 6.01.

Synthesis of Neutral Rhodium(III) Complex [RhI$_2$(COMe)(CO)$_2$($N_2C_3H_4$)] (7d). In situ characterization of a CO bridge-splitting reaction: To a CD_2Cl_2 solution of **6d** (100 mg, 0.098 mmol) under stirring was fed bubbling CO (1 bar) for 2 min. The reaction mixture turned dark red and was analyzed by FT-IR spectroscopy. For $^{13}C\{^1H\}$ NMR characterization, the reaction was carried out with **6d-^{13}CO** under a ^{13}CO atmosphere. When not kept under a CO atmosphere, the reaction was reversible and dimer **6d** was recovered. FT-IR (ν_{CO}, ν_{COMe}, cm^{-1}): 2155.6 (w), 2073.2 (s), 1735.9 (s) (CH_2Cl_2). **7d-^{13}CO**. ^1H NMR (298 K, CD_2Cl_2, 400.13 MHz, ppm): δ 8.58 (s, 1H, ring N=C*H*N−CH_3), 7.95 (d, 1H, ring NC*H*=CHN−CH_3, $^3J_{H-H}$ = 1.2 Hz), 6.98 (d, 1H, ring NCH=C*H*N−CH_3, $^3J_{H-H}$ = 1.2 Hz), 3.84 (s, 3H, ring NCH=CHN−CH_3), 2.82 (s, 3H, COCH_3). $^{13}C\{^1H\}$ NMR (298 K, 100.62 MHz, CD_2Cl_2, ppm): δ 210.2 (d, 1C, [Rh]−*C*OMe, $^1J_{C-Rh}$ = 21.6 Hz), 183.4 (d, 2C, [Rh]−*C*O, $^1J_{C-Rh}$ = 58.5 Hz), 145.0 (s, 1C, ring N=*C*HN−CH_3), 134.5 (s, 1C, ring NCH=*C*HN−CH_3), 120.5 (s, 1C, ring NCH=*C*HN−CH_3), 47.4 (s, 1C, COCH_3), 34.7 (s, 1C, ring NCH=CHN−CH_3).

Synthesis of Neutral Rhodium(III) Complex [RhI$_2$(COMe)(CO)($N_2C_3H_4$)$_2$] (8e). To a dichloromethane solution (V = 10 mL) of **6e** (100 mg, 0.100 mmol) under stirring was added a solution of 2 mol equiv of ligand **e** in dichloromethane (V = 2 mL). The reaction mixture was vigorously stirred at room temperature for 6 h. After solvent removal under vacuum, compound **8e** obtained was washed with ether and extracted with pentane, dried under vacuum, and stored under argon at 255 K prior to use. Red microcrystalline product (yield 94%). X-ray-quality crystals were obtained in pentane at 255 K. FT-IR (ν_{CO}, ν_{COMe}, cm^{-1}): 2082.5, 1698.9, 1677.4 (CH_2Cl_2). ^1H NMR (298 K, CD_2Cl_2, 400.13 MHz, ppm): δ 11.24 (br s, 1H, ring1 N−N*H*−CH), 8.06 (br s, 2H, ring1 C*H*=N−NH−C*H*), 7.74 (s, 1H, ring2 C*H*=N−NH−CH), 7.05 (s, 1H, ring2 CH=N−NH−C*H*),

dx.doi.org/10.1021/ic2019988 | *Inorg. Chem.* 2012, 51, 8670−8685

6.54 (s, 1H, ring1 NH−CH=C*H*), (s, 1H, ring2 NH−CH=C*H*), 3.09 (s, 3H, [Rh]−CO*CH*$_3$), 1.58 (br s, 1H, ring2 N−N*H*−CH). ^{13}C{^{1}H} NMR (298 K, 100.62 MHz, CD_2Cl_2, ppm): δ 219.3 (dd 1C, [Rh]−COMe, $^1J_{COMe-Rh}$ = 19.7 Hz, $^2J_{C-C}$ = 3.7 Hz), 182.5 (d, 1C, [Rh]−*C*O, $^1J_{C-Rh}$ = 59.8 Hz), 141.7 (s, 2C, ring1 *C*H=N−NH, ring2 *C*H=N−NH), 130.3 (s, 2C, ring1 N−NH−*C*H, ring2 N−NH−*C*H), 107.7 (s, 1C, ring1 NH−CH=*C*H), 107.2 (s, 1C, ring2 NH−CH=*C*H), 51.5 (s 1C, [Rh]−CO*C*H$_3$). Anal. Calcd for $C_9H_{11}IN_4O_2Rh$: C, 24.72; H, 2.52; N, 12.82. Found: C, 24.74; H, 2.54; N, 12.75.

Characterization of Ionic Rhodium Complexes. *[RhI$_2$(CO)$_2$](HNMeEt$_2$).* FT-IR (ν_{CO}, cm^{-1}): 2065.4, 1995.4 (CH_2Cl_2), 2057.8, 1986.9 (CH_3I). ^{1}H NMR (298 K, 300.180 MHz, acetone-d_6, ppm): δ 7.45 (br s, 1H, >NH, *H*N(CH$_3$)(CH$_2$CH$_3$)$_2$), 3.50 (q, 2H, >CH$_2$, HN(CH$_3$)(C*H*$_2$CH$_3$)$_2$, J_{H-H} = 7.2 Hz), 3.28 (q, 2H, >CH$_2$, HN(CH$_3$)(C*H*$_2$CH$_3$)$_2$, J_{H-H} = 6.9 Hz), 3.15 (s, 3H, −CH$_3$, HN(C*H*$_3$)(CH$_2$CH$_3$)$_2$), 1.35 (tt, 3H, −CH$_3$, HN(CH$_3$)(CH$_2$C*H*$_3$)$_2$, J_{H-N} = 2.1 Hz, J_{H-H} = 7.5 Hz), 1.31 (t, 3H, −CH$_3$, HN(CH$_3$)(CH$_2$C*H*$_3$)$_2$, J_{H-H} = 7.2 Hz). ^{13}C{^{1}H} NMR (298 K, 75.480 MHz, acetone-d_6, ppm): δ 184.05 (d, [Rh]−CO, J_{C-Rh} = 71.9 Hz), 59.27 (t, >CH$_2$, HN(CH$_3$)(CH$_2$CH$_3$)$_2$, J_{C-N} = 2.9 Hz), 49.88 (t, −CH$_3$, HN(*C*H$_3$)(CH$_2$CH$_3$)$_2$, J_{C-N} = 4.0 Hz), 43.30 (br s, >CH$_2$, HN(CH$_3$)(CH$_2$CH$_3$)$_2$), 11.23 (s, −CH$_3$, HN(CH$_3$)(CH$_2$CH$_3$)$_2$), 8.1 (s, −CH$_3$, HN(CH$_3$)(CH$_2$CH$_3$)$_2$).

[RhI$_2$(CO)$_2$](NH$_2$Et$_2$). FT-IR (ν_{CO}, cm^{-1}): 2069.9, 2000.6 (CH_2Cl_2), 2065.0, 1996.0 (CH_3I). ^{1}H NMR (298 K, 300.18 MHz, CD_2Cl_2, ppm): δ 7.06 (br t, 2H, NH, N*H*$_2$Et$_2$, J_{H-N} = 38.1 Hz), 3.34 (q, 4H, >CH$_2$, NH$_2$(C*H*$_2$CH$_3$)$_2$, J_{H-H} = 6.9 Hz), 1.57 (t, 6H, −CH$_3$, N(H$_2$CH$_2$C*H*$_3$)$_2$, J_{H-H} = 7.2 Hz). ^{13}C{^{1}H} NMR (298 K, 75.480 MHz, CD_2Cl_2, ppm): δ 182.70 (d, [Rh]−CO, J_{C-Rh} = 69.2 Hz), 43.55 (s, >CH$_2$, H$_2$N(CH$_2$CH$_3$)$_2$), 11.49 (s, −CH$_3$, H$_2$N(CH$_2$CH$_3$)$_2$).

[RhI$_2$(CO)$_2$](SMeEt$_2$). FT-IR (ν_{CO}, cm^{-1}): 2062.9, 1992.2 (CH_2Cl_2), 2058.4, 1987.7 (CH_3I). ^{1}H NMR (298 K, 300.13 MHz, CD_2Cl_2, ppm): δ 3.57 (m, 4H, >CH$_2$, S(CH$_3$)(C*H*$_2$CH$_3$)$_2$), 3.06 (s, 3H, −CH$_3$, S(C*H*$_3$)(CH$_2$CH$_3$)$_2$), 1.57 (t, 6H, −CH$_3$, S(CH$_3$)(CH$_2$C*H*$_3$)$_2$, J_{H-H} = 7.5 Hz). ^{13}C{^{1}H} NMR (298 K, 75.468 MHz, CD_2Cl_2, ppm): δ 183.28 (d, [Rh]−CO, J_{C-Rh} = 71.7 Hz), 35.81 (s, >CH$_2$, S(CH$_3$)(CH$_2$CH$_3$)$_2$), 22.32 (s, −CH$_3$, S(CH$_3$)(CH$_2$CH$_3$)$_2$), 9.32 (s, −CH$_3$, S(CH$_3$)(CH$_2$CH$_3$)$_2$).

[RhI$_2$(μ-I)(CO)(COMe)]$_2$(H$_2$NEt$_2$)$_2$. Red powder poorly soluble in CH_2Cl_2. FT-IR (ν_{CO}, ν_{COMe}, cm^{-1}): 2075.7, 2068.2, 1723.3, 1699.1 (CH_2Cl_2), 2066.4, 1715.2 (CH_3I). ^{1}H NMR (298 K, 300.18 MHz, CD_2Cl_2, ppm): δ 7.44 (br t, 4H, NH, N*H*$_2$Et$_2$, J_{H-N} = 40.2 Hz), 3.34 (q, 8H, >CH$_2$, NH$_2$(C*H*$_2$CH$_3$)$_2$, J_{H-H} = 7.2 Hz), 3.15 (s, 6H, −CH$_3$, [Rh]−CO*CH*$_3$), 1.54 (t, 12H, −CH$_3$, NH$_2$(CH$_2$C*H*$_3$)$_2$, J_{H-H} = 7.2 Hz). Anal. Calcd for $C_{14}H_{30}I_6N_2O_4Rh_2$ (%): C, 13.37; H, 2.40; N, 2.23. Found: C, 13.51; H, 2.49; N, 2.31.

[RhI$_2$(μ-I)(CO)(COMe)]$_2$(HNMeEt$_2$)$_2$. Red powder. FT-IR (ν_{CO}, ν_{COMe}, cm^{-1}): 2069.2, 1719.3 (CH_2Cl_2), 2061.4, 1696.1 (CH_3I). ^{1}H NMR (298 K, 300.131 MHz, CD_2Cl_2, ppm): δ 8.24 (br s, 2H, NH, N(*H*)(CH$_3$)(CH$_2$CH$_3$)$_2$, 3.47 (q, 4H, >CH$_2$, N(H)(CH$_3$)(C*H*$_2$CH$_3$)$_2$, J_{H-H} = 7.5 Hz), 3.21 (q, 4H, >CH$_2$, N(H)(CH$_3$)(C*H*$_2$CH$_3$)$_2$, J_{H-H} = 7.2 Hz), 3.16 (s, 6H, −CH$_3$, N(H)(C*H*$_3$)(CH$_2$CH$_3$)$_2$, 3.15 (br s, 6H, [Rh]−CO*CH*$_3$), 1.55 (t, 6H, −CH$_3$, N(H)(CH$_3$)(CH$_2$C*H*$_3$)$_2$, J_{H-H} = 7.2 Hz), 1.48 (tt, 6H, −CH$_3$, N(H)(CH$_3$)(CH$_2$C*H*$_3$)$_2$, J_{H-N} = 2.1 Hz, J_{H-H} = 7.5 Hz). ^{13}C{^{1}H} NMR (298 K, 75.468 MHz, CD_2Cl_2, ppm): δ not observed ([Rh]−*C*OCH$_3$), 186.08 (d, [Rh]−*C*O, J_{C-Rh} = 76.3 Hz), 182.11 (d, [Rh]−*C*OCH$_3$, J_{C-Rh} = 71.4 Hz), 60.01 (t, >CH$_2$, N(H)(CH$_3$)(CH$_2$CH$_3$)$_2$, J_{C-N} = 2.9 Hz), 50.77 (t, −CH$_3$, N(H)(CH$_3$)(CH$_2$CH$_3$)$_2$, J_{C-N} = 4.2 Hz), 49.49 (br, ([Rh]−COCH$_3$), 42.40 (s, >CH$_2$, N(H)(CH$_3$)(CH$_2$CH$_3$)$_2$, 10.98 (s, −CH$_3$, N(H)(CH$_3$)(CH$_2$CH$_3$)$_2$, 8.45 (s, −CH$_3$, N(H)(CH$_3$)(CH$_2$CH$_3$)$_2$. Anal. Calcd for $C_{16}H_{34}I_6N_2O_4Rh_2$: C, 14.95; H, 2.67; N, 2.18. Found: C, 15.01; H, 2.63; N, 2.25.

[RhI$_2$(μ-I)(CO)(COCH$_3$)]$_2$[MeSEt$_2$)$_2$]. Red powder (yield 85%). FT-IR (ν_{CO}, ν_{COMe}, cm^{-1}): 2067.0, 1718.9 (CH_2Cl_2), 2076.1, 2065.2, 1720.0 (CH_3I). ^{1}H NMR (298 K, 300.13 MHz, CD_2Cl_2, ppm): δ 3.55 (m, 8H, >CH$_2$, S(CH$_3$)(C*H*$_2$CH$_3$)$_2$), 3.15 (br s, 6H, −CH$_3$, [Rh]−CO*CH*$_3$), 3.06 (s, 6H, −CH$_3$, S(C*H*$_3$)(CH$_2$CH$_3$)$_2$), 1.58 (t, 12H, −CH$_3$, S(CH$_3$)(CH$_2$C*H*$_3$)$_2$), J_{H-H} = 7.2 Hz). ^{13}C{^{1}H} NMR (298 K, 100.623 MHz, CD_2Cl_2, ppm): δ 210.69 (br s, [Rh]−*C*OCH$_3$), 183.31 (d, [Rh]−*C*O, J_{C-Rh} = 72.2 Hz), 182.09 31 (d, [Rh]−*C*O, J_{C-Rh} = 70.0 Hz), 49.53 (br s, −CH$_3$, [Rh]−COCH$_3$), 35.74 (s, >CH$_2$, S(CH$_3$)(CH$_2$CH$_3$)$_2$), 21.83 (s, −CH$_3$, S(*C*H$_3$)(CH$_2$CH$_3$)$_2$), 9.10 (s, −CH$_3$, S(CH$_3$)(CH$_2$CH$_3$)$_2$). Anal. Calcd for $C_{16}H_{32}I_6O_4Rh_2S_2$: C, 14.56; H, 2.44. Found: C, 14.70; H, 2.58.

X-ray Structure Determination. X-ray structures were determined on an Oxford Diffraction Xcalibur CCd diffractometer. The crystallographic data were collected at low temperature, 180(2) K, on a Bruker Kappa APEX II diffractometer (**3e**, **3f**, **4d**, **4e**, and **6e**) or a Gemini Oxford Diffraction diffractometer (**3a**, **3d**, **4a**, **4f**, **6d$_1$**, **6d$_2$**, and **8e**), both equipped with an Oxford Cryosystems Cryostream cooler device and using Mo Kα radiation (λ = 0.71073 Å). The structures were solved by direct methods using *SHELXS-97*[40] or *SIR92*,[41] and all non-hydrogen atoms were refined anisotropically using the least-squares method on F^2 with the aid of the program *SHELXL-97*.[42] The drawing of molecules was performed with the program *ORTEP*.[43]

Kinetic Measurements. In a typical experiment, to a Schlenk tube containing the complex was added MeI (5 mL), which was previously adjusted at the desired temperature. Immediately after mixing under stirring, the stopwatch was switched on and a sample of the reaction solution was rapidly transferred by syringe to an IR cell (CaF_2 window, 1.00 mm path length) fitted with a thermostatted jacket and placed in the sample compartment. FT-IR spectra (4.0 cm^{-1} resolution) were scanned in the region 4000−450 cm^{-1} and saved at regular time intervals using spectrum software *TIMEBASE*. Absorbance (A_t) versus time data for the appropriate $\nu_{(CO)}$ frequencies were extracted by subtracting the solvent spectrum. Kinetic measurements were made by following the decay of the lower antisymmetric frequency $\nu_{(CO)}$ band of the rhodium(I) starting complexes **4**. The pseudo-first-order rate constants were found from the gradient of the plot of ln(A_t) versus time where A_t is the absorbance at the time t.

■ ASSOCIATED CONTENT

Ⓢ Supporting Information

X-ray crystallographic data in CIF format, Eyring plots and relative activation parameter determinations ($H^‡$, $S^‡$, $G^‡$, and E_a) for NMR exchange processes, IR-monitored kinetic CH_3I oxidative addition data, kinetic data for **4a** and **4c**−**4h**, crystallographic data and structure rifinement, FT-IR and ATR-IR spectra, and NMR data/selected rhodium(I) and rhodium(III) NMR spectra, and selected VT-NMR spectra. This material is available free of charge via the Internet at http://pubs.acs.org.

■ AUTHOR INFORMATION

Corresponding Author

*E-mail: duc.nguyen@ensiacet.fr (D.H.N.), philippe.kalck@ensiacet.fr (P.K.).

Notes

The authors declare no competing financial interest.

■ ACKNOWLEDGMENTS

Yannick Coppel, Christian Bijani (LCC-Toulouse), and Alain Moreau (LCC-Toulouse) are gratefully acknowledged for technical assistance and helpful discussions in NMR and elemental analyses, respectively. We are indebted to Jean-Claude Daran (LCC-Toulouse) for further fruitful discussions concerning hydrogen-bonding analyses on the X-ray crystal structures.

■ REFERENCES

(1) (a) Haynes, A. In *Topics in Organometallic Chemistry*; Beller, M., Ed.; Springer-Verlag: Berlin, 2006; p 179. (b) Haynes, A. *Adv. Catal.* **2010**, *53*, 1. (c) Torrence, P. In *Applied Homogeneous Catalysis with Organometallic Compounds*; Cornils, B.; Herrmann, W. A.; Eds.; Wiley-VCH: Weinheim, Germany, 2002; p 104.

(2) (a) Forster, D.; Dekleva, T. W. *Adv. Catal.* **1986**, *34*, 81. (b) Lassauque, N.; Davin, T.; Nguyen, D. H.; Adcock, R. J.; Coppel, Y.; Le Berre, C.; Serp, P.; Maron, L.; Kalck, P. *Inorg. Chem.* **2012**, *51*, 4.

(3) Some selected examples: (a) Paulik, F. E.; Hershman, A.; Knox, W. R.; Roth, J. F. (to Monsanto). U.S. Patent 4,690,912, 1987. (b) Brodzki, D.; Leclere, C.; Denise, B.; Pannetier, G. *Bull. Soc. Chim. Fr.* **1976**, 61. (c) Rankin, J.; Poole, A. D.; Benyei, A. C.; Cole-Hamilton, D. J. *Chem. Commun.* **1997**, 1835. (d) Rankin, J.; Benyei, A. C.; Poole, A. D.; Cole-Hamilton, D. J. *J. Chem. Soc., Dalton Trans.* **1999**, 3771. (e) Bader, A.; Lindner, E. *Coord. Chem. Rev.* **1991**, *108*, 27. (f) Dutta, D. K.; Woollins, J. D.; Slawin, A. M. Z.; Konwar, D.; Das, P.; Sharma, M.; Bhattacharyya, P.; Aucott, S. M. *Dalton Trans.* **2003**, 2674. (g) Wegman, R. W.; Abatjoglou, A. G. (to Union Carbide Corp.). U.S. Patent 4,670,570, 1987. (h) Wegman, R. W.; Abatjoglou, A. G.; Harrison, A. M. *J. Chem. Soc., Chem. Commun.* **1987**, 1891. (i) Baker, M. J.; Giles, M. F.; Orpen, A. G.; Taylor, M. J.; Watt, R. J. *J. Chem. Soc., Chem. Commun.* **1995**, 197. (j) Baker, M. J.; Dilworth, J. R.; Sunley, J. G.; Wheatley, N. (to BP Chemicals). European Patent EU0632006, 1995. (k) Dilworth, J. R.; Miller, J. R.; Wheatley, N.; Baker, M. J.; Sunley, J. G. *J. Chem. Soc., Chem. Commun.* **1995**, 1579. (l) Conifer, C. M.; Law, D. J.; Sunley, G. J.; White, A. J. P.; Britovsek, G. J. P. *Organometallics* **2011**, *30*, 4060. (m) Gonsalvi, L.; Adams, H.; Sunley, G. J.; Ditzel, E.; Haynes, A. *J. Am. Chem. Soc.* **2002**, *124*, 13597. (n) Thomas, C. M.; Süss-Fink, G. *Coord. Chem. Rev.* **2003**, *243*, 125. (o) Gonsalvi, L.; Adams, H.; Sunley, G. J.; Ditzel, E.; Haynes, A. *J. Am. Chem. Soc.* **1999**, *121*, 11233.

(4) Martin, H. C.; James, N. H.; Aitken, J.; Gaunt, J. A.; Adams, H.; Haynes, A. *Organometallics* **2003**, *22*, 4451.

(5) Frech, C. M.; Milstein, D. *J. Am. Chem. Soc.* **2006**, *128*, 12434.

(6) Wells, J. R.; Haynes, A.; Adams, H. *Book of Abstracts P-251*; 17th International Symposium on Homogeneous Catalysis, Poznań, Poland, July 4–9, 2010; p 330.

(7) Gonsalvi, L.; Gaunt, J. A.; Adams, H.; Castro, A.; Sunley, G. J.; Haynes, A. *Organometallics* **2003**, *22*, 1047.

(8) (a) Borah, B. J.; Deb, B.; Sarmah, P. P.; Saikia, K.; Khound, P. P.; Dutta, D. K. *Inorg. Chim. Acta* **2011**, *370*, 117. (b) Sarmah, P. P.; Deb, B.; Borah, B. J.; Fuller, A. L.; Slawin, A. M. Z.; Woollins, J. D.; Dutta, D. K. *J. Organomet. Chem.* **2010**, *695*, 2603. (c) Borah, B. J.; Deb, B.; Sarmah, P. P.; Dutta, D. K. *J. Mol. Catal. A: Chem.* **2010**, *319*, 66. (d) Dutta, D. K.; Chutia, P.; Sarmah, B. J.; Borah, B. J.; Deb, B.; Woollins, J. D. *J. Mol. Catal. A: Chem.* **2009**, *300*, 29. (e) Srinivasan, A.; Toganoh, M.; Niino, T.; Osuka, A.; Furuta, H. *Inorg. Chem.* **2008**, *47*, 11305. (f) Sarmah, B. J.; Borah, B. J.; Deb, B.; Dutta, D. K. *J. Mol. Catal. A: Chem.* **2008**, *289*, 95. (g) Kumari, N.; Sarmah, B. J.; Dutta, D. K. *J. Mol. Catal. A: Chem.* **2007**, *266*, 260. (h) Kumari, N.; Sharma, M.; Chutia, P.; Dutta, D. K. *J. Mol. Catal. A: Chem.* **2004**, *222*, 53. (i) Kumari, N.; Sharma, M.; Das, P.; Dutta, D. K. *Appl. Organomet. Chem.* **2002**, *16*, 258. (j) Dutta, D. K.; Singh, M. M. *Transition Met. Chem.* **1994**, *19*, 290.

(9) (a) Conifer, C. M.; Taylor, R. A.; Law, D. J.; Sunley, G. J.; White, A. J. P.; Britovsek, G. J. P. *Dalton Trans.* **2011**, *40*, 1031. (b) Conifer, C. M.; Law, D. J.; Sunley, G. J.; Haynes, A.; Wells, J. R.; White, A. J. P.; Britovsek, G. J. P. *Eur. J. Inorg. Chem.* **2011**, 3511.

(10) (a) Jang, K.; Kim, H. J.; Son, S. U. *Chem. Mater.* **2010**, *22*, 1273. (b) Jang, K.; Jung, I. G.; Nam, H. J.; Jung, D. Y.; Son, S. U. *J. Am. Chem. Soc.* **2009**, *131*, 12046. (c) Bitterwolf, T. E.; Newell, J. D.; Carver, C. T.; Addleman, R. S.; Linehan, J. C.; Fryxell, G. *Inorg. Chim. Acta* **2004**, *357*, 3001. (d) Bitterwolf, T. E.; Scallorn, W. B.; Bays, J. T.; Weiss, C. A.; Linehan, J. C.; Franz, J.; Poli, R. *J. Organomet. Chem.* **2002**, *652*, 95. (e) Gao, H.; Angelici, R. J. *New J. Chem.* **1999**, *23*, 633. (f) Vallarino, L. M.; Sheargold, S. W. *Inorg. Chim. Acta* **1979**, *36* (2), 243. (g) Balch, A. L.; Cooper, R. D. *J. Organomet. Chem.* **1979**, *169* (1), 97. (h) Fougeroux, P.; Denise, B.; Bonnaire, R.; Pannetier, G. *J. Organomet. Chem.* **1973**, *60* (2), 375. (i) Bonati, F.; Ugo, R. *J. Organomet. Chem.* **1967**, *7* (1), 167–80. (j) Lawson, D. N.; Wilkinson, G. *J. Chem. Soc.* **1965**, 1900.

(11) (a) Song, Q.; Yuan, G.; Shao, S.; Yan, F.; Ling, C.; Qian, Q.; Cao, H. Chinese Patent CN 101367051 A 20090218, 2009. (b) Bonati, F.; Oro, L. A.; Pinillos, M. T.; Tejel, C.; Apreda, M. C.; Foces-Foces, C.; Cano, F. H. *J. Organomet. Chem.* **1989**, *369*, 253. (c) Palensky, F. J.; Siedle, A. R. *Eur. Pat. Appl.* EP 61241 A1 19820929, 1982.

(12) (a) Cano, M.; Campo, J. A.; Heras, J. V.; Lafuente, J.; Rivas, C.; Pinilla, E. *Polyhedron* **1995**, *14*, 1139. (b) Cano, F. H.; Foces-Foces, C.; Oro, L. A.; Pinillos, M. T.; Tejel, C. *Inorg. Chim. Acta* **1987**, *128*, 75. (c) Decker, M. J.; Fjeldsted, D. O. K.; Stobart, S. R.; Zaworotko, M. J. *Chem. Commun.* **1983**, *24*, 1525.

(13) Haynes, A.; Mann, B. E.; Morris, G. E.; Maitlis, P. M. *J. Am. Chem. Soc.* **1993**, *115*, 4093.

(14) For pK_a values, see: Catalan, J.; Elguero, J. *J. Chem. Soc., Perkin Trans.* **1983**, 1869.

(15) Cotton, F. A. *Chemical Applications of Group Theory*; John Wiley & Sons: New York, 1990.

(16) Tolman, C. A. *Chem. Rev.* **1977**, *77*, 313.

(17) (a) Petrucci, M. G. L.; Lebuis, A. M.; Kakkar, A. K. *Organometallics* **1998**, *17*, 4966. (b) Garralda, M. A.; Hernandez, R.; Pinilla, E.; Torres, M. R. *J. Organomet. Chem.* **1999**, *586*, 150.

(18) This short distance is more likely due to the somewhat closed N–H–Cl angle of 106.81° induced by solid-state packing constraints so that it is not considered as a proper hydrogen-bonding interaction. See: Jeffrey, G. A.; Saenger, W. *Hydrogen Bonding in Biological Structures*; Springer: Berlin, 1991.

(19) (a) Borkett, N. F.; Bruce, M. I. *J. Organomet. Chem.* **1974**, *65*, C51. (b) Bushnell, G. W.; Dixon, K. R.; Eadie, D. T.; Stobart, S. R. *Inorg. Chem.* **1981**, *20*, 1545. (c) Atwood, J. L.; Dixon, K. R.; Eadie, D. T.; Stobart, S. R.; Zaworotko, M. J. *Inorg. Chem.* **1983**, *22*, 774. (d) Heaton, B. T.; Jacob, C.; Sampanthar, J. T. *Dalton Trans.* **1998**, 1403. (e) Brück, A.; Ruhland, K. *Organometallics* **2009**, *28*, 6383. (f) Litchman, W. M. *J. Am. Chem. Soc.* **1979**, *101*, 545.

(20) Zobi, F. *Inorg. Chem.* **2010**, *49*, 10370.

(21) (a) Mann, K. R.; Gordon, J. G., II; Gray, H. B. *J. Am. Chem. Soc.* **1975**, *97*, 3553. (b) Mann, K. R.; Lewis, N. S.; Williams, R. M.; Gray, H. B.; Gordon, J. G., II. *Inorg. Chem.* **1978**, *17*, 828. (c) Bera, J. K.; Dunbar, K. R. *Angew. Chem., Int. Ed.* **2002**, *41*, 4453.

(22) For **4a**, the N–H···I distance of 2.900 Å and the N–H–I angle of 116.98°, which is larger than that in the chloro analogue **3a**, are still not considered as intramolecular interactions.

(23) Garcia-Seijo, M. I.; Habtemariam, A.; Fernandez-Anca, D.; Parsons, S.; Garcia-Fernandez, M. E. Z. *Anorg. Allg. Chem.* **2002**, *628*, 1075.

(24) H_a slightly shifted downfield (7.77 ppm) in comparison with H_b (7.72 ppm) because of the electron-withdrawing effect of the closer {RhI(CO)$_2$} moiety.

(25) For **4c** and **4d**, the coalescence temperature was not reached even when working at room temperature in CD_2Cl_2 (low boiling point). Thus, ^{1}H and ^{13}C{^{1}H} VT-NMR experiments for determination of the activation parameters were measured in a CD_3OD solvent.

(26) For the further less basic thiophene ligand, the formation of the split monomeric complex [RhI(CO)$_2$(thiophene)] starting from **2** and 2 equiv of ligand was not detected by FT-IR spectroscopy, which indicates a much higher labile character of this S-heterocyclic ligand.

(27) $^1J_{NRh}$ values for **4e** and **4f** have not been determined because of the large signals obtained. For **4f**, a 1.8 ppm δ^{15}_{N1-Rh} shift toward higher fields was observed, whereas δ(^{15}N2–Me) is not affected in comparison with those of the corresponding free ligand **f** (δ^{15}_{N1} = −152.1 ppm; δ^{15}_{N2} = −178.9 ppm).

(28) (a) Fabrello, A.; Dinoi, C.; Perrin, L.; Kalck, P.; Maron, L.; Urrutigoïty, M.; Dechy-Cabaret, O. *Magn. Reson. Chem.* **2010**, *48*, 448. (b) Nguyen, D. H.; Lauréano, H.; Jugé, S.; Kalck, P.; Daran, J. C.; Coppel, Y.; Urrutigoïty, M.; Gouygou, M. *Organometallics* **2009**, *28*, 6288.

(29) Haynes, A.; Maitlis, P. M.; Stanbridge, I. A.; Haak, S.; Pearson, J. M.; Adams, H.; Bailey, N. A. *Inorg. Chim. Acta* **2004**, *357*, 3027.

(30) The addition of 2 equiv of **a** to the solution of **5** in dichloromethane at room temperature induced the reductive elimination to generate the identified rhodium(I) complexes **4a**, [Rh(CO)$_2$I$_2$][NH$_2$Et$_2$], and *N*,*N*-diethylacetamide.

(31) Adams, H.; Bailey, N. A.; Mann, B. E.; Manuel, C. P.; Spencer, C. M.; Kent, A. G. *Dalton Trans.* **1988**, 489.

(32) Even at very low temperature (193 K), static structures in solution were still not observed, presumably because of both intra- and intermolecular fluxional processes among at least 18 possible isomers.[34]

(33) Under such reaction conditions, reductive elimination took place to give back the rhodium(I) species **4d** and CH_3COI, which further reacted with traces of adventitious water to give acetic acid (δ_{CH_3COOH} = 175.9 ppm) and HI. For **4d**, the broad $^{13}C\{^1H\}$ NMR carbonyl signal at 180 ppm observed at room temperature is presumably due to fast exchange with free labeled ^{13}CO dissolved in the medium. Acetic anhydride has also been detected ($\delta_{(CH_3CO)_2O}$ = 166.5 ppm) presumably because of the reaction of CH_3COI with AcOH under insufficient water concentration. A similar reaction has previously been observed for $[RhI_2(COMe)_2(CO)]_n$.[32] In parallel, a small doublet centered at 179.3 ppm ($^1J_{CO-Rh}$ = 49.0 Hz) has been assigned speculatively to $[RhI_3(CO)_2(\mathbf{d})]$, which was formed via HI oxidative addition upon **4d**. This reactivity has been explored in our group for the corresponding anionic $[RhI_2(CO)_2]^-$, affording $[RhI_4(CO)_2]^-$, for which CO resonated as expected at higher field: δ_{CO} = 173.1 ppm, $^1J_{CO-Rh}$ = 48.1 Hz [countercation: PPN^+ = bis(triphenylphosphoranylidene)ammonium].

(34) Adamson, G. W.; Daly, J. J.; Forster, D. *J. Organomet. Chem.* **1974**, *71*, 17.

(35) Ion, L.; Nieto, S.; Perez, J.; Riera, L.; Riera, V.; Diaz, J.; Lopez, R.; Anderson, K. M.; Steed, J. W. *Inorg. Chem.* **2011**, *50*, 8524.

(36) Unlike the observation or isolation of intermediate methylrhodium(III) species starting from $[RhI_2(CO)_2]^-$ or [RhI(CO)(P−L)],[3,13] we did not detect any corresponding neutral $[RhI_2(Me)(CO)_2(\mathbf{L})]$ from **4c**−**4g**, even in neat CH_3I. This can be explained first by the lower electron density on the rhodium center brought by amine ligand L, resulting in the lower polarization of both [Rh]−Me and [Rh]−CO bonds and, consequently, favors the CO migratory insertion. Moreover, the steric hindrance of N-heterocycles can also have a positive impact on this step. The similar implication of steric effects on both oxidative addition and insertion reactions has been previously observed by Haynes et al. for rhodium(I) N-heterocyclic carbene and α-diimine complexes.[4,7]

(37) In separate experiments, $[RhI_2(CO)_2]^-$ complexes with $[NH_2Et_2]^+$ and $[NHMeEt_2]^+$ countercations as well as their corresponding dimeric acetylrhodium(III) complexes $[RhI_2(\mu\text{-}I)(COMe)(CO)]_2^{2-}$ have been synthesized with the respective CH_3I oxidative addition reaction rate constants ($k_{298\ K} \times 10^{-5}$) of 62.0 and 19.6 s^{-1}. On the other hand, the kinetic curves for CH_3I oxidative addition to **4a** and **4h** are complicated. It appears that both the successive and competitive reactions have to be studied to understand the reaction kinetics. In the later stages of the reaction of **4a** where the corresponding ionic $[RhI_2(CO)_2]^-$ species is clearly observed, the rate constant $k_{298\ K} \times 10^{-5}$ estimated from the consumption of starting **4a** is 67 s^{-1}, which is very close to that of $[RhI_2(CO)_2]^-[NHMeEt_2]^+$. Similarly, the $[RhI_2(CO)_2]^-[SMeEt_2]$ and $[RhI_2(\mu\text{-}I)(COMe)(CO)]_2[SMeEt_2]_2$ complexes have also been prepared, and the CH_3I oxidative addition rate ($k_{298\ K} \times 10^{-5}$ = 97.1 s^{-1}) is close to that of $[RhI(CO)_2(SEt_2)]$, which is consistent with the exclusive involvement of $[RhI_2(CO)_2]^-$.

(38) McCleverty, J.; Wilkinson, G. *Inorg. Synth.* **1966**, *8*, 214.

(39) Burger, S.; Therrien, B.; Süss-Fink, G. *Acta Crystallogr.* **2003**, *E59*, i53.

(40) Sheldrick, G. M. *Acta Crystallogr.* **1990**, *A46*, 467.

(41) Altomare, A.; Cascarano, G.; Giacovazzo, C.; Guagliardi, A. *J. Appl. Crystallogr.* **1993**, *26*, 343.

(42) Sheldrick, G. M. *SHELXL-97, Program for Crystal Structure Refinement*; University of Göttingen: Göttingen, Germany, 1997.

(43) Farrugia, L. J. *J. Appl. Crystallogr.* **1997**, *30*, 565.